Diffusion in channeled structures. III. Quantum corrections induced by lattice vibrations

Benoit Palmieri and David Ronis
Department of Chemistry, McGill University, 801 Sherbrooke Ouest, Montréal, Québec, Canada H3A 2K6
(Received 8 January 2007; published 27 July 2007)

For large energy barrier systems the lattice vibrations can play an important role in the diffusion of a guest component inside channeled structures. Here, quantum corrections to the guest diffusion are studied within a semiclassical framework in which the guest behaves classically and the lattice quantum mechanically. The permeability is expressed in terms of correlation functions that are calculated using path integrals. Forward-backward path integrals for propagators are combined, and, using the Martin-Siggia-Rose formalism [Phys. Rev. A. **8**, 423 (1973)], are transformed into a set of generalized Langevin equations that reduce to the classical equation of motion at high temperatures. The random initial conditions to these equations are specified by the density matrix from which an approximate expression for the quantum mechanical potential of mean force is derived. The quantum potential of mean force and activation energy obtained for the guest inside the lattice is slightly higher than the one for the fully classical system, and the diffusion of the guest in the quantum lattice is slower compared to its fully classical counterpart. The macroscopic intrinsic permeability of α-quartz towards neon is reported, $P'_{\mathrm{qtm}}(300\ \mathrm{K})=9.91\times10^{8}$ s/(mkg) within the semiclassical approximation and is lower than $P'_{\mathrm{class}}(300\ \mathrm{K})=1.26\times10^{9}$ s/(mkg) obtained in the classical case at 300 K for the same potential model.

DOI: 10.1103/PhysRevE.76.011124 PACS number(s): 05.60.−k, 66.30.−h, 05.30.−d

I. INTRODUCTION

In two recent papers [1,2], hereafter referred to as papers I and II, we studied the intracrystalline diffusion of a guest inside selected zeolites. There, we used the formalism initially developed by Ronis and Vertenstein [3] to calculate the permeability through a channeled crystalline interface of finite thickness separating two bulk regions that contain the guest component at different chemical potentials. The advantage of using this formalism is that it is fully microscopic in the sense that the permeability is obtained from the integration of a space-dependent Onsager diffusion coefficient which, in turn, is calculated from simulations of specific guest time-correlation functions. In papers I and II, we compared our method with transition state theory (TST), which is often used to describe the diffusion in these types of systems [4–6] and where it is assumed that the guest diffusion follows one or more reaction coordinates. Within our formalism, we were able to test the underlying assumptions of transition state theory which where shown to be inappropriate for more open channels.

A major part of our work in papers I and II was to understand the role that lattice vibrations play in the diffusion process. Many earlier studies of diffusion in channeled structures used standard molecular dynamics (MD) with a frozen lattice [7–9] to simulate the motion of the guest. Following these studies, the motion of the crystal atoms was included by simulating the vibrational motion of a relatively small number of lattice atoms [4–6,10]. The role of the lattice vibrations on the guest diffusion had been studied, before us, by Kopelevich and Chang [11] and by Suffritti and coworkers [12–14]. In Ref. [11], only the motion of the guest was simulated from a generalized Langevin equation (GLE) where the energy exchange with the lattice was described by dissipative (memory) and random terms which were approximated phenomenologically using a simple one parameter model for the memory function.

In papers I and II we used a model similar to that of Ref. [11]. In our formalism, the motion of the guest *and* selected target atoms (the only ones that interact directly with the guest) was explicitly simulated using a set of GLE's. The energy exchange with the infinite bath (the part of the crystal that does not interact directly with the guest) was included by the dissipative and random force terms that typically arise in GLE and that are related by generalized Einstein-Nyquist relations or the second fluctuation-dissipation theorem (see, e.g., Ref. [15]). The periodicity of the lattice and the approximation that the crystal is harmonic allowed us to compute the memory function exactly. This memory function was then fitted to a general simple function that allowed us to include the memory and noise terms in the equations of motion for the target atoms. As shown in papers I and II, the success of our procedure is that the approximate memory function we use is exact for long and short times and hence, it accurately reproduces the full crystal vibrational density of states. Within this framework the role of the lattice vibrations on the diffusion process was studied. In paper I, the guest (xenon) was diffusing in a crystalline zeolite that has wide channels (Theta-1). There, we found that lattice vibrations did not affect the motion of the guest insofar as the permeability is concerned. On the other hand, in paper II, we explored the diffusion of argon in α-quartz, a crystal with very narrow channels. For this system, we found that the flexibility and lattice vibrational motion played a significant role in the guest dynamics, most importantly, on the free energy landscape.

For systems such as the one studied in paper II, where lattice vibrations play a significant role in the diffusion, another question naturally arises, namely, should we treat the problem, or at least parts of it, quantum mechanically? After

 ©2007 The American Physical Society

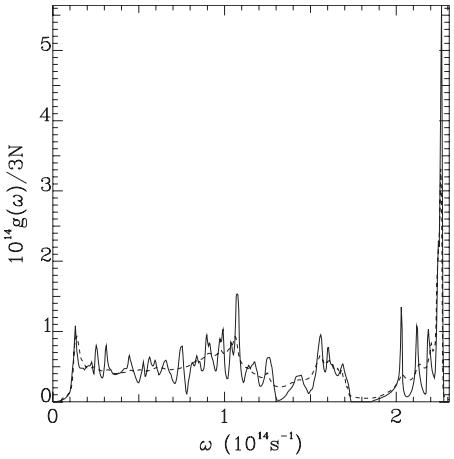

FIG. 1. The exact density of states (full line) for α-quartz is compared with the one obtained from our approximate form for the memory function (dashed line), cf. Eq. (4.35).

all, it is well known that most vibrational modes in typical crystals are not thermally excited at room temperature. Specifically, $\omega^* \equiv \hbar\omega/k_BT$ is the dimensionless parameter that characterizes how quantum mechanical a vibrational mode with frequency ω at temperature T is. The vibration is classical when $\omega^* \ll 1$ and quantum mechanical when $\omega^* \gg 1$. At room temperature, $\omega^*=1$ when $\omega=0.393\times10^{14}$ s^{-1}. A typical vibrational density of states is shown in Fig. 1, and shows that roughly 75% of the vibrational modes are in the quantum regime at 300 K.

In this paper, we will use an entirely different formalism based on path integrals to approximately include the quantum mechanical nature of the lattice. The goal is to calculate the quantum corrections to the potential of mean force of the guest in the presence of the quantum lattice, to obtain the quantum corrections to the space-dependent Onsager diffusion coefficient and, ultimately, to see what kind of correction arises at the macroscopic level, i.e., on the permeability.

The paper is divided as follows, in Sec. II we show how the permeability is expressed in terms of Kubo averages and we recall what types of correlations have to be calculated in order to obtain the space-dependent Onsager diffusion coefficient. In Sec. III we describe the path integral approach that allows us to obtain the required correlations semiclassically. In particular, a closed form expression for the density matrix is obtained and we show how forward-backward path integrals approximately define a set of second order differential equations that can be turned in a stochastic initial value problem. We explicitly show how, in the classical limit, these equations reduce to the classical generalized Langevin equations of motions obtained in papers I and II. In Sec. IV, we show how to implement the formalism developed in Sec. III. More precisely, we describe how the potential of mean force is obtained from our expression for the density matrix and explain how the new (nonclassical) terms are calculated numerically using the theory of defects, Brillouin zone sums and contour integrations. We then describe how these techniques can be further used to simulate the nonclassical terms in the generalized Langevin equations.

In Sec. V, we apply our theory to the study of neon in α-quartz. We first show that our formalism is exact in the absence of the guest, and then report the main results of this paper; specifically, quantum corrections slightly increase the potential of mean force of the guest inside the crystal, the difference increasing with reduced temperature. In addition, we show that the lattice effectively vibrates more (the velocity correlations have larger amplitudes) when quantum mechanics is included and, for this system, this results in a slower diffusion for the guest and a permeability which is about 25% smaller compared to the classical one. Section VI contains a discussion and concluding remarks.

II. THE TIME-CORRELATION FUNCTION FORM OF THE PERMEABILITY

As was discussed in papers I and II (and references therein), the permeability intrinsic to the material is given by

$$\frac{1}{P'} = \frac{1}{\beta}\int_{-d}^{d} dz \frac{1}{D(z)}, \tag{2.1}$$

where $\beta \equiv 1/k_BT$, $2d$ is the width of the interface separating the two bulk regions containing the guest and

$$D(z) \equiv \frac{1}{A}\int_0^\infty dt \int d\mathbf{r} \int d\mathbf{r}'_\parallel \langle \mathbf{J}_z^\dagger(\mathbf{r},t)\mathbf{J}_z^\dagger(\mathbf{r}')\rangle, \tag{2.2}$$

is a space-dependent Onsager diffusion coefficient. In this last expression, $\mathbf{r}$ and $\mathbf{r}'$ are spatial coordinates, t is the time, and A is the area of the crystalline interface. In addition, $\mathbf{J}_z^\dagger(\mathbf{r}) \equiv \exp[i(1-\mathcal{P})\mathcal{L}t](1-\mathcal{P})\mathbf{J}_z(\mathbf{r})$ is the z component of the dissipative part of the guest diffusion current, where $\mathcal{P}$ is a projection operator (see below) and $\mathcal{L}$ is the Liouville operator. The integral over $\mathbf{r}_\parallel$, i.e., (x,y), is a consequence of the fact that the average current through the interface was chosen to lie along the z axis.

In papers I and II, $\langle \mathbf{J}_z^\dagger(\mathbf{r},t)\mathbf{J}_z^\dagger(\mathbf{r}')\rangle$ in Eq. (2.2) is a simple correlation function that, modulo effects associated with the daggers, can be easily evaluated from classical molecular dynamics simulations. Quantum mechanically, the expression for $D(z)$ is slightly modified from Eq. (2.2): the current fields $\mathbf{J}^\dagger$ become operators $\hat{\mathbf{J}}^\dagger$ (henceforth, we use "$\hat{O}$" to denote a quantum mechanical operator) and the classical correlations are replaced by Kubo averages [16] defined as

$$\langle \hat{A}(t)\hat{B}\rangle_K \equiv \int_0^1 d\lambda \, \mathrm{Tr}[\hat{A}(t)e^{-\lambda\beta\hat{H}}\hat{B}e^{\lambda\beta\hat{H}}\hat{\rho}], \tag{2.3}$$

where $\hat{H}$ is the Hamiltonian operator, Tr is a quantum mechanical trace, and $\hat{\rho} \equiv e^{-\beta\hat{H}}/Q$ is the density matrix, with the partition function, $Q \equiv \mathrm{Tr}[e^{-\beta\hat{H}}]$. For a recent review where Kubo averages are used to study quantum liquids, see Ref. [17].

The quantum or classical mechanical expressions for $D(z)$ are not particularly useful in the above form without a prescription that takes care of the effects that the projection operators (i.e., the daggers) have on the current operators and on their time dependence. For the classical case, Vertenstein and Ronis [3,18] obtained a relation, expressed in terms of standard correlation functions, that approximately accounts

for the projection operators. They used a projection operator formalism [19,20] with the projection operator

$$\mathcal{P}\mathsf{A} \equiv \langle \mathsf{A}N\rangle * \langle NN\rangle^{-1} * N, \tag{2.4}$$

where the N is the fluctuation in number density of the guest component and an asterisk denotes any spatial integrations. Note that $\langle NN\rangle^{-1}$ is not an algebraic inverse of the $\langle NN\rangle$ correlation function, rather it is the solution to $\int d\mathbf{r}_1\langle N(\mathbf{r})N(\mathbf{r}_1)\rangle\langle N(\mathbf{r}_1)N(\mathbf{r}')\rangle^{-1}=\delta(\mathbf{r}-\mathbf{r}')$. With this in hand, they showed, assuming infinite dilution for the guest in the crystal, that $D(z)$ could be accurately approximated by

$$D(z) = \frac{n_\infty \int_0^\infty dt\, \langle v_{G,z}(t) v_{G,z}\rangle_{z(t=0)=z} e^{-\beta W(z)}}{1 + \int_0^\infty dt\, \langle \beta F[z(t)] v_{G,z}\rangle_{z(t=0)=z}}, \tag{2.5}$$

where n_∞ is the number density in the bulk, $v_{G,z}$ is the z component of the guest velocity, $W(z)$ and $F(z)$ are, respectively, the plane average potential of mean force and the mean force. Specifically,

$$e^{-\beta W(z)} \equiv \frac{1}{A}\int d\mathbf{r}_\parallel e^{-\beta W(\mathbf{r})}, \tag{2.6}$$

where $\mathbf{r}$ is the guest position, $W(\mathbf{r})$ is the usual potential of mean force, and $F(z)\equiv -\partial W(z)/\partial z$. All correlations in Eq. (2.5) are evaluated conditional to the z component of the guest position being initially equal to z (and is indicated by the subscripts on the averages). Finally, note that this derivation uses the fact that $\langle N(\mathbf{r})N(\mathbf{r}')\rangle = n_\infty \delta(\mathbf{r}-\mathbf{r}')e^{-\beta W(\mathbf{r})}$ and further assumes that $D(z)/e^{-\beta W(z)}$ is approximately constant near the barrier top (this approximation is exact for Smoluchowski diffusion processes [21]).

For our problem, an appropriate choice of projection operator is defined by Eq. (2.4) after the correlations have been replaced by Kubo averages and the variables A and N by operators, see Ref. [22]. By repeating the steps that led to Eq. (2.5), see Refs. [3,18], it is easy to show that

$$\begin{aligned}\langle \hat{\mathbf{J}}(\mathbf{r},t)\hat{\mathbf{J}}(\mathbf{r}')\rangle_K = \langle \hat{\mathbf{J}}^\dagger(\mathbf{r},t)\hat{\mathbf{J}}^\dagger(\mathbf{r}')\rangle_K - \int_0^t d\tau \int d\mathbf{r}_1 \\ \times \int d\mathbf{r}_2 \langle \hat{\mathbf{J}}^\dagger(\mathbf{r},\tau)\hat{\mathbf{J}}^\dagger(\mathbf{r}_1)\rangle_K \frac{\partial}{\partial \mathbf{r}_1} \\ \times (\langle \hat{N}(\mathbf{r}_1)\hat{N}(\mathbf{r}_2)\rangle_K^{-1}\langle \hat{N}(\mathbf{r}_2,t-\tau)\hat{\mathbf{J}}(\mathbf{r}')\rangle_K.\end{aligned} \tag{2.7}$$

Note that unlike the classical case, here, at infinite guest dilution, $\langle \hat{N}(\mathbf{r}_1)\hat{N}(\mathbf{r}_2)\rangle_K \neq \langle \hat{N}(\mathbf{r}_1)\hat{N}(\mathbf{r}_2)\rangle = n(\mathbf{r}_1)\delta(\mathbf{r}_1-\mathbf{r}_2)$.

Hence, a solution for the irreversible current correlations $\langle \hat{\mathbf{J}}^\dagger(\mathbf{r},t)\hat{\mathbf{J}}^\dagger(\mathbf{r}')\rangle_K$ requires that the various Kubo average correlations that appear in Eq. (2.7) be computed and the integral equation solved. The next section shows how any of these Kubo averages can be obtained within a semi-classical picture that relies on the fact that the guest dynamics is slow compared to the vibrations. In particular, for the types of averages that appear in Eq. (2.7), $D(z)$ is obtained from an expression identical to Eq. (2.5), but with a corrected potential of mean force and a new set of dynamical equations, used to calculate the desired correlations; these take into account the effect of the quantum degrees of freedom (i.e., the crystal vibrations).

In what follows, we will work with the anticommutator correlations defined as

$$\langle\{\hat{A}(t),\hat{B}\}\rangle \equiv \mathrm{Tr}[(\hat{A}(t)\hat{B}+\hat{B}\hat{A}(t))\hat{\rho}]. \tag{2.8}$$

This anticommutator correlations can then be used to obtain the Kubo transform using the standard relation [16]

$$\langle \hat{A}(t)\hat{B}\rangle_K = \int_{-\infty}^\infty dt'\, \gamma(t-t')\frac{1}{2}\langle\{\hat{A}(t'),\hat{B}\}\rangle, \tag{2.9}$$

where $\gamma(t)$ is most easily represented spectrally as

$$\gamma(t) \equiv \frac{1}{2\pi}\int_{-\infty}^\infty d\omega\, e^{i\omega t}\frac{\tanh(\beta\hbar\omega/2)}{\beta\hbar\omega/2}. \tag{2.10}$$

III. EVALUATION OF ANTICOMMUTATOR CORRELATION FUNCTIONS USING PATH INTEGRALS

As in papers I and II, we assume that the guest component is anharmonically coupled to a limited number of atoms in the crystal, which we call target atoms. These target atoms are allowed to further interact with themselves and with any other atoms of the macroscopic crystal that do not interact with the guest directly, the so-called bath atoms (note that this last assumption can be relaxed to allow harmonic interactions between guest and bath). The interaction between any two crystal atoms is assumed to be harmonic. This model is described by the following Hamiltonian:

$$\begin{aligned}\hat{H} \equiv \frac{\hat{p}_g^2}{2m_g} + \frac{1}{2}\hat{\mathsf{P}}_t^T\mathsf{M}_{tt}^{-1}\hat{\mathsf{P}}_t + \frac{1}{2}\hat{\mathsf{P}}_b^T\mathsf{M}_{bb}^{-1}\hat{\mathsf{P}}_b + V(\hat{\mathbf{r}}_g,\hat{\mathsf{R}}_t) + \frac{1}{2}\hat{\mathsf{R}}_t^T\mathsf{K}_{tt}\hat{\mathsf{R}}_t \\ + \hat{\mathsf{R}}_t^T\mathsf{K}_{tb}\hat{\mathsf{R}}_b + \frac{1}{2}\hat{\mathsf{R}}_b^T\mathsf{K}_{bb}\hat{\mathsf{R}}_b,\end{aligned} \tag{3.1}$$

where $\hat{\mathbf{p}}_g$ and $\hat{\mathbf{r}}_g$ are the guest momentum and position operators, $\hat{\mathsf{P}}_{t,b}$ and $\hat{\mathsf{R}}_{t,b}$ are vectors of the target/bath momentum and position operators, K with subscript tt, tb, and bb denotes a block of the force constant matrix, and the superscript T indicates a matrix transpose.

We now turn to the evaluation of the anti-commutator correlation function. This correlation function can be formally written in the coordinate representation as

$$\begin{aligned}\frac{1}{2}\langle\{\hat{A}(t),\hat{B}\}\rangle = \frac{1}{2}\int d\mathsf{R}_1 \int d\mathsf{R}_2 \int d\mathsf{R}_3 \{K_-(\mathsf{R}_1,\mathsf{R}_2;t) \\ \times \hat{A}(\mathsf{R}_2)K_+(\mathsf{R}_2,\mathsf{R}_3;t)\hat{B}(\mathsf{R}_3) + \hat{B}(\mathsf{R}_1) \\ \times K_-(\mathsf{R}_1,\mathsf{R}_2;t)\hat{A}(\mathsf{R}_2)K_+(\mathsf{R}_2,\mathsf{R}_3;t)\}\frac{\rho(\mathsf{R}_3,\mathsf{R}_1)}{Q}\end{aligned} \tag{3.2}$$

for diagonal $\hat{A}$ and $\hat{B}$ operators in coordinate space, where

$\mathsf{R}_i \equiv (\mathbf{r}_g^T, \mathsf{R}_t^T, \mathsf{R}_b^T)_i^T$, for $i=1,2,3$, and where, using bra-ket notation

$$K_{\pm}(\mathsf{R}_1,\mathsf{R}_2;t) \equiv \langle \mathsf{R}_1 | e^{\mp i\hat{H}t/\hbar} | \mathsf{R}_2 \rangle, \tag{3.3}$$

$$\rho(\mathsf{R}_1,\mathsf{R}_2) \equiv \langle \mathsf{R}_1 | e^{-\beta\hat{H}} | \mathsf{R}_2 \rangle, \tag{3.4}$$

and

$$Q \equiv \int d\mathsf{R}\, \rho(\mathsf{R},\mathsf{R}) \tag{3.5}$$

is the partition function. Note that the operator $\hat{B}(\mathsf{R}_1)$ in the second term of the right-hand side of Eq. (3.2) only acts on $K_-(\mathsf{R}_1,\mathsf{R}_2;t)$ and not on $\rho(\mathsf{R}_3,\mathsf{R}_1)$.

A. The density matrix

We first focus on the density matrix, $\rho(\mathsf{R}_1,\mathsf{R}_2)$. It can be written in terms of path integrals as [23]

$$\rho(\mathsf{R}_1,\mathsf{R}_2) = \int \mathcal{D}[\mathsf{R}(\tau)] e^{-(1/\hbar)\mathcal{A}}, \tag{3.6}$$

where the Euclidean action is given by

$$\mathcal{A} \equiv \int_0^{\beta\hbar} d\tau \left[\frac{m_g \dot{r}_g^2}{2} + \frac{\dot{\mathsf{R}}_t^T \mathsf{M}_{tt} \dot{\mathsf{R}}_t}{2} + \frac{\dot{\mathsf{R}}_b^T \mathsf{M}_{bb} \dot{\mathsf{R}}_b}{2} + V(\mathbf{r}_g,\mathsf{R}_t) + \frac{1}{2}\mathsf{R}_t^T \mathsf{K}_{tt} \mathsf{R}_t + \mathsf{R}_t^T \mathsf{K}_{tb} \mathsf{R}_b + \frac{1}{2}\mathsf{R}_b^T \mathsf{K}_{bb} \mathsf{R}_b \right], \tag{3.7}$$

where the time argument was omitted for all position variables and where $\dot{\mathbf{r}}_g(\tau) \equiv d\mathbf{r}_g/d\tau$, etc. All paths are constrained to start at R_1 and end at R_2. We will now use, for the first but not the last time, the fact that the guest is slow at room temperature and higher and we will argue, as in Ref. [23], that the position of the guest barely changes in the complex time interval, $\beta\hbar$. Effectively, for this path integral, we treat the guest as a free particle evolving in a constant potential. Therefore, we set $\mathbf{r}_g = \mathbf{r}_g^{(0)}$ (to be specified later) in the last equation and, as in papers I and II, we Taylor expand $V(\mathbf{r}_g^{(0)},\mathsf{R}_t)$ with respect to the crystal coordinates around $\mathsf{R}_t = \mathsf{R}_t^{(0)}(\mathbf{r}_g^{(0)})$, a point at which there is no net force on the crystal atoms; i.e., where

$$\mathsf{K}_{\text{eff}} \mathsf{R}_t^{(0)} = -\frac{\partial V(\mathbf{r}_g^{(0)},\mathsf{R}_t^{(0)})}{\partial \mathsf{R}_t} \tag{3.8}$$

and $\mathsf{R}_b^{(0)} = -\mathsf{K}_{bb}^{-1}\mathsf{K}_{bt}\mathsf{R}_t^{(0)}$, where $\mathsf{K}_{\text{eff}} \equiv \mathsf{K}_{tt} - \mathsf{K}_{tb}\mathsf{K}_{bb}^{-1}\mathsf{K}_{bt}$. It is easy to show that the best choice of $\mathbf{r}_g^{(0)}$ is the midpoint $(\mathbf{r}_{1,g} + \mathbf{r}_{2,g})/2$, in that it makes the first corrections in $\hbar$ for the guest vanish. As in papers I and II, the terms in the Taylor expansion for $V(\mathbf{r}_g^{(0)},\mathsf{R}_t)$ above second order are neglected.

Within these approximations, the only path integrals that have to be evaluated are a simple free propagator for the guest and standard harmonic potential path integrals for the crystal (see, e.g., Refs. [23,24]). The manipulations are standard and the final expression for the density matrix is

$$\rho(\mathsf{R}_1,\mathsf{R}_2) = \left[\left(\frac{m_g}{2\pi\beta\hbar^2} \right)^3 \det\left(\frac{\Xi(\mathsf{D})}{2\pi\hbar} \right) \right]^{1/2} \exp\Bigg(-\beta V(\mathbf{r}_g^{(0)},\mathsf{R}_t^{(0)}) - \frac{m_g \mathbf{y}_g^2}{2\beta\hbar^2} - \beta\frac{(\mathsf{R}_t^{(0)})^T \mathsf{K}_{\text{eff}} \mathsf{R}_t^{(0)}}{2} - \frac{(\mathsf{R}_{1,c} - \mathsf{R}_c^{(0)})^T \Lambda(\mathsf{D}) (\mathsf{R}_{1,c} - \mathsf{R}_c^{(0)})}{2\hbar} - \frac{(\mathsf{R}_{2,c} - \mathsf{R}_c^{(0)})^T \Lambda(\mathsf{D}) (\mathsf{R}_{2,c} - \mathsf{R}_c^{(0)})}{2\hbar} + \frac{(\mathsf{R}_{1,c} - \mathsf{R}_c^{(0)})^T \Xi(\mathsf{D}) (\mathsf{R}_{2,c} - \mathsf{R}_c^{(0)})}{\hbar} \Bigg), \tag{3.9}$$

where $\mathsf{R}_c \equiv (\mathsf{R}_t^T, \mathsf{R}_b^T)^T$, $\mathbf{y}_g \equiv \mathbf{r}_{2,g} - \mathbf{r}_{1,g}$,

$$\Lambda(\mathsf{D}) \equiv \mathsf{M}^{1/2} (\tilde{\mathsf{K}} + \tilde{\mathsf{D}})^{1/2} \coth(\beta\hbar [\tilde{\mathsf{K}} + \tilde{\mathsf{D}}]^{1/2}) \mathsf{M}^{1/2}, \tag{3.10}$$

$$\Xi(\mathsf{D}) \equiv \mathsf{M}^{1/2} (\tilde{\mathsf{K}} + \tilde{\mathsf{D}})^{1/2} \operatorname{csch}(\beta\hbar [\tilde{\mathsf{K}} + \tilde{\mathsf{D}}]^{1/2}) \mathsf{M}^{1/2}, \tag{3.11}$$

and K is a matrix defined in the crystal subspace containing the harmonic force constants. The $\Lambda(\mathsf{D})$ and $\Xi(\mathsf{D})$ are matrices defined in the full crystal subspace and are functions of the curvature matrix

$$\mathsf{D} \equiv \left. \frac{\partial^2 V(\mathbf{r}_g^{(0)},\mathsf{R}_t)}{\partial \mathsf{R}_t\, \partial \mathsf{R}_t} \right|_{\mathsf{R}_t = \mathsf{R}_t^{(0)}}, \tag{3.12}$$

which, by assumption, is nonzero only in the target subspace and which depends on the guest position. Finally, henceforth, a tilde over any matrix indicates that it has been mass scaled, e.g., $\tilde{\mathsf{K}} \equiv \mathsf{M}_c^{-1/2} \mathsf{K} \mathsf{M}_c^{-1/2}$, where $\mathsf{M} \equiv \text{diag}(m_g, \mathsf{M}_t, \mathsf{M}_b)$.

A guest potential of mean force can be defined, as in papers I and II, in terms of the diagonal part of the reduced density matrix as

$$e^{-\beta W(\mathbf{r}_g)} \equiv \frac{\rho_R(\mathbf{r}_g)}{Q_{\text{harmonic}}} \left(\frac{m_g}{2\pi\beta\hbar^2} \right)^{-3/2}, \tag{3.13}$$

where

$$\rho_R(\mathbf{r}_g) \equiv \int d\mathsf{R}_c \rho(\mathsf{R},\mathsf{R}), \tag{3.14}$$

and where Q_{harmonic} is the partition function of the crystal decoupled from the guest. This definition makes $W(\mathbf{r}_g)$ zero when the guest is far from the crystal. Using this definition, we find that

$$W(\mathbf{r}_g) = V(\mathbf{r}_g,\mathsf{R}_t^{(0)}) + \frac{1}{2}(\mathsf{R}_t^{(0)})^T \mathsf{K}_{\text{eff}} \mathsf{R}_t^{(0)} + \Delta W(\mathbf{r}_g), \tag{3.15}$$

where all the temperature dependent terms are in

$$\Delta W(\mathbf{r}_g) \equiv \frac{k_B T}{2} \ln\left(\frac{\det[(\Lambda(\mathsf{D}) - \Xi(\mathsf{D}))\Xi(\mathsf{D})^{-1}]}{\det[(\Lambda(0) - \Xi(0))\Xi(0)^{-1}]} \right). \tag{3.16}$$

The first two terms on the right-hand side of Eq. (3.15) appear in the classical potential of mean force obtained in papers I and II. The temperature dependence of the potential of mean force is different here than what we had in papers I and II (where an expansion in powers of temperature results) and arises because of the quantum nature of the crystal vibrations (for a numerical comparison, see Sec. V A). In the high temperature limit all the vibrational modes are excited, and Eq. (3.15) is easily shown to reduce to the classical expression

$$W_{\mathrm{class}}(\mathbf{r}_g) = V(\mathbf{r}_g, \mathsf{R}_t^{(0)}) + \frac{1}{2}(\mathsf{R}_t^{(0)})^T \mathsf{K}_{\mathrm{eff}} \mathsf{R}_t^{(0)} + \frac{k_B T}{2} \ln[\det(1 + \mathsf{K}_{\mathrm{eff}}^{-1}\mathsf{D})]. \tag{3.17}$$

In the derivation of Eq. (3.9) the guest was assumed to behave like a free-particle in the time interval $\beta\hbar$. Other techniques that approximately include quantum mechanical effects in the calculations of partition functions and density matrices have been developed, and, in principle, could have been used above. Of these, the variational approach of Feynman and Kleinert [25,26] and its extensions (see, e.g., Refs. [26–28]) is very accurate, but is only useful for nonsingular potentials. Ermakov, Butayev, and Spiridonov [29] suggested an approximate expression, exact for harmonic potentials, which gives the right high-temperature (classical) limit and which can be applied to any potential. This method was improved by Mak and Andersen [30], Cao and Berne [31], and by Chao and Andersen [32]. We give the details of an application of these methods to our problem in the Appendix and show in Sec. V that similar results are obtained, at least for experimentally relevant temperatures. (The experiments that measure the diffusion of gases through crystals are rarely performed at or below room temperature.)

As a final comment, note that many authors, in their calculations of the density matrix, assume that, at time $t=0$, the system (here, guest and target) and the bath are decoupled [33,34]. Here, this approximation is clearly inappropriate. The guest has two effects on the crystal degrees of freedom. First, it modifies the force constant matrix in the *tt* block, but also shifts the oscillator centers, even in the bath. This last effect would be absent if the bath was decoupled.

B. Forward-backward path integrals and connection with MSR

Next, we obtain a similar semiclassical approximation for the real-time propagators $K_{\pm}(\mathsf{R}_1, \mathsf{R}_2; t)$. Each of these propagators is written as

$$K_{\pm}(\mathsf{R}_1, \mathsf{R}_2; t) = \int \mathcal{D}[\mathsf{R}_{\pm}(\tau)] e^{\pm(i/\hbar)S_{\pm}}, \tag{3.18}$$

where $K_{\pm}$ is the forward (backward) propagator defined in terms of the action

$$S_{\pm} \equiv \int_0^t d\tau \left(\frac{1}{2} m_g \dot{r}_{g,\pm}^2 + \frac{1}{2} \dot{\mathsf{R}}_{c,\pm}^T \mathsf{M}_{cc} \dot{\mathsf{R}}_{c,\pm} - V(\mathbf{r}_{g,\pm}, \mathsf{R}_{t,\pm}) - \frac{1}{2} \mathsf{R}_{c,\pm}^T \mathsf{K} \mathsf{R}_{c,\pm} \right), \tag{3.19}$$

where, for the + (−) propagator, all paths start (end) at R_2 and end (start) at R_1. We then have to consider these path integrals in terms of a semiclassical picture consistent with our treatment of the density matrix in the previous section. The formalism that we will use to evaluate these propagators is inspired from the work of Schmid *et al.* [35,36] and of Kleinert and Shabanov [33] who obtained quantum Langevin equations for simpler systems.

Here, rather than considering the two propagators individually, we will work with the combination $K_-(\mathsf{R}_1, \mathsf{R}_2; t)\hat{A}(\mathsf{R}_2)K_+(\mathsf{R}_2, \mathsf{R}_3; t)$ appearing in Eq. (3.2). We first realize that the operator $\hat{A}(\mathsf{R}_2)$ only acts on the end point of the positive time propagator. With this in mind, we will replace R_2 in the argument of $\hat{A}$ and K_+ by Z and, after the operator $\hat{A}(\mathsf{Z})$ has acted on the combination $K_-(\mathsf{R}_1, \mathsf{R}_2; t)K_+(\mathsf{Z}, \mathsf{R}_3; t)$, we will set Z back to R_2. This combination of forward-backward path integrals is rewritten in terms of sums and differences of the forward and backward path variables

$$K_-(\mathsf{R}_1, \mathsf{R}_2; t)K_+(\mathsf{Z}, \mathsf{R}_3; t) = \int \mathcal{D}[\mathsf{X}(\tau)]\mathcal{D}[\mathsf{Y}(\tau)] \exp\left(\frac{i}{\hbar} \int_0^t d\tau \left[m_g \dot{\mathbf{x}}_g \cdot \dot{\mathbf{y}}_g + \dot{\mathsf{X}}_c^T \mathsf{M}_{cc} \dot{\mathsf{Y}}_c - V\left(\mathbf{x}_g + \frac{\mathbf{y}_g}{2}, \mathsf{X}_c + \frac{\mathsf{Y}_c}{2} \right) + V\left(\mathbf{x}_g - \frac{\mathbf{y}_g}{2}, \mathsf{X}_c - \frac{\mathsf{Y}_c}{2} \right) - \mathsf{X}_c^T \mathsf{K}_{cc} \mathsf{Y}_c \right] \right), \tag{3.20}$$

where $\mathsf{X} \equiv (\mathsf{R}_+ + \mathsf{R}_-)/2$ and $\mathsf{Y} \equiv \mathsf{R}_+ - \mathsf{R}_-$. Note that the boundary condition for $\mathsf{Y}(t) = \mathsf{Z} - \mathsf{R}_2$ becomes equal to zero when Z is set back to R_2.

We use the same approximations as above and Taylor expand the potential in the action in Y. All the even terms in Y cancel and we keep only the linear ones, neglecting terms of order $O(\mathsf{Y}^3)$. Again, for the guest, this is justified because, for the temperatures considered, the paths are localized around the classical trajectory which, as will be shown below, is given by the classical equations of motion for $\mathbf{x}_g(\tau)$ and $\mathsf{X}_c(\tau)$. For the crystal variables, the expansion is again approximately valid since, for any forward or backward path, the crystal position will not deviate strongly from their mean because of the strength of the harmonic part of the potential. After this expansion is carried out, the argument in the exponential becomes linear in Y. This results in a path integral which closely resembles that which is obtained in the Martin-Siggia-Rose (MSR) formalism [37,38] that represents stochastic processes as path integrals. This suggest that we should be able to revert the MSR formalism and simulate the path integrals from a set of stochastic differential equations.

We now show that this transformation can indeed be carried for our system. This derivation follows that of Jensen's [38] derivation of MSR in reverse. We start by writing the path integrals in their discretized form and make use of the approximations described in the preceding paragraph. This gives,

$$K_-(\mathsf{R}_1,\mathsf{R}_2;t)K_+(\mathsf{Z},\mathsf{R}_3;t) \approx \lim_{N\to\infty}\left\{\left(\frac{m_g}{2\pi\hbar\epsilon}\right)^{3(N+1)}\det\left(\frac{\mathsf{M}_c}{2\pi\hbar\epsilon}\right)^{N+1}\int\prod_{j=1}^{N}d\mathsf{X}_j d\mathsf{Y}_j \exp\left[\frac{i\epsilon}{\hbar}\sum_{m=0}^{N}\left(\frac{m_g(\mathbf{x}_{g,m+1}-\mathbf{x}_{g,m})\cdot(\mathbf{y}_{g,m+1}-\mathbf{y}_{g,m})}{\epsilon^2}\right.\right.\right.$$
$$\left.\left.\left.+\frac{(\mathsf{X}_{c,m+1}-\mathsf{X}_{c,m})^T\mathsf{M}_{cc}(\mathsf{Y}_{c,m+1}-\mathsf{Y}_{c,m})}{\epsilon^2}+\mathbf{F}_g(\mathbf{x}_{g,m},\mathsf{X}_{t,m})\cdot\mathbf{y}_{g,m}+\mathsf{F}_t(\mathbf{x}_{g,m},\mathsf{X}_{t,m})^T\mathsf{Y}_{t,m}-\mathsf{X}_{c,m}^T\mathsf{K}_{cc}\mathsf{Y}_{c,m}\right)\right]\right\}, \tag{3.21}$$

where $\epsilon\equiv t/N$, the $j=0$ and $j=N+1$ subscripts represent the boundary conditions on the paths at $\tau=0$ and $\tau=t$, respectively, and where the forces are defined by

$$\mathbf{F}_g(\mathbf{x}_{g,m},\mathsf{X}_{t,m}) \equiv -\frac{\partial V(\mathbf{x}_{g,m},\mathsf{X}_{t,m})}{\partial \mathbf{x}_{g,m}} \tag{3.22}$$

and

$$\mathsf{F}_t(\mathbf{x}_{g,m},\mathsf{X}_{t,m}) \equiv -\frac{\partial V(\mathbf{x}_{g,m},\mathsf{X}_{t,m})}{\partial \mathsf{X}_{t,m}} \tag{3.23}$$

as usual.

Clearly, the fact that we have dropped all cubic terms and higher in $\mathsf{Y}(\tau)$ allows us to perform all the $\mathbf{y}_{g,j}$ and $\mathsf{Y}_{c,j}$ integrals for $j=1\cdots N$, which gives a product of delta functions that can be trivially manipulated to give

$$K_-(\mathsf{R}_1,\mathsf{R}_2;t)K_+(\mathsf{Z},\mathsf{R}_3;t) \approx \lim_{N\to\infty}\left\{\left(\frac{m_g}{2\pi\hbar\epsilon}\right)^{3}\det\left(\frac{\mathsf{M}_c}{2\pi\hbar\epsilon}\right)\int\prod_{j=1}^{N}d\mathsf{X}_j\prod_{m=1}^{N}\left[\delta\left(\mathbf{x}_{g,m+1}-2\mathbf{x}_{g,m}+\mathbf{x}_{g,m-1}-\frac{\epsilon^2}{m_g}\mathbf{F}_g(\mathbf{x}_{g,m},\mathsf{X}_{t,m})\right)\delta\left(\mathsf{X}_{c,m+1}\right.\right.\right.$$
$$\left.\left.-2\mathsf{X}_{c,m}+\mathsf{X}_{c,m-1}-\frac{\epsilon^2}{\mathsf{M}_{cc}}[\mathsf{F}_t(\mathbf{x}_{g,m},\mathsf{X}_{t,m})-\mathsf{K}_{cc}\mathsf{X}_{c,m}]\right)\right]\exp[-i(m_g/\hbar\epsilon)(\mathbf{x}_{g,1}-\mathbf{x}_{g,0})\cdot\mathbf{y}_{g,0}+i(m_g/\hbar\epsilon)$$
$$\left.\times(\mathbf{x}_{g,N+1}-\mathbf{x}_{g,N})\cdot\mathbf{y}_{g,N+1}-i(\mathsf{X}_{c,1}-\mathsf{X}_{c,0})^T(\mathsf{M}_{cc}/\hbar\epsilon)\mathsf{Y}_{c,0}+i(\mathsf{X}_{c,N+1}-\mathsf{X}_{c,N})^T(\mathsf{M}_{cc}/\hbar\epsilon)\mathsf{Y}_{c,N+1}]\right\}. \tag{3.24}$$

In order to proceed, note that after the operator $\hat{A}(\mathsf{Z})$ acts on $K_-(\mathsf{R}_1,\mathsf{R}_2;t)K_+(\mathsf{Z},\mathsf{R}_3;t)$ and after Z is set back to R_2, we obtain a function, $A(\mathbf{x}_g(t),\mathbf{v}_g(t))$ that multiplies $K_-(\mathsf{R}_1,\mathsf{R}_2;t)K_+(\mathsf{R}_2,\mathsf{R}_3;t)$, where $\mathbf{x}_g(t)$ and $\mathbf{v}_g(t)$ are, respectively, the guest final position and velocity [the final velocity is defined by $\mathbf{v}_g(t)\equiv(\mathbf{x}_{g,N+1}-\mathbf{x}_{g,N})/\epsilon$] [39]. We will show examples of this function for specific choices of the operator $\hat{A}$ in the following section.

We now use the fact that the final position phase vector, $\mathsf{R}_2=(\mathbf{x}_{g,N+1}^T,\mathsf{X}_{t,N+1}^T,\mathsf{X}_{b,N+1}^T)^T$ is integrated over all possible R_2 in the anticommutator expression [see Eq. (3.2)] to realize that, in the $N\to\infty$ limit, the product of delta functions combined with the integrations over X_2, $\mathsf{X}_3,\ldots,\mathsf{X}_N$ forces $\mathsf{X}_{N+1}=\mathsf{X}(t)=\mathsf{R}_2$ to be the solution of the initial value problem

$$m_g\frac{d^2\mathbf{x}_g}{dt^2}=\mathbf{F}_g(\mathbf{x}_g,\mathsf{X}_t), \tag{3.25a}$$

$$\mathsf{M}_{tt}\frac{d^2\mathsf{X}_t}{dt^2}=\mathsf{F}_t(\mathbf{x}_g,\mathsf{X}_t)-\mathsf{K}_{tt}\mathsf{X}_t-\mathsf{K}_{tb}\mathsf{X}_b, \tag{3.25b}$$

and

$$\mathsf{M}_{bb}\frac{d^2\mathsf{X}_b}{dt^2}=-\mathsf{K}_{bb}\mathsf{X}_b-\mathsf{K}_{bt}\mathsf{X}_t, \tag{3.25c}$$

with initial position $\mathsf{X}(0)=\mathsf{X}_0=(\mathsf{R}_1+\mathsf{R}_3)/2$ and velocities $\dot{\mathsf{X}}(0)=\mathsf{V}(0)=(\mathsf{X}_1-\mathsf{X}_0)/\epsilon$ (recall that the integrals over X_1 were not performed yet). The remaining integrations in the anticommutator expression (3.2) are over R_1, R_3, and X_1. A simple change of variables allows us to reexpress the anticommutator as

$$\frac{1}{2}\langle\{\hat{A}(t),\hat{B}\}\rangle = \frac{1}{2}\left(\frac{m_g}{2\pi\hbar}\right)^3 \det\left(\frac{\mathsf{M}_{cc}}{2\pi\hbar}\right)\int d\mathsf{X}(0)d\mathsf{V}(0)d\mathsf{Y}\left[e^{-i(m_g/\hbar)\mathbf{v}_g(0)\cdot\mathbf{y}_g - i\mathsf{V}_c(0)^T(\mathsf{M}_{cc}/\hbar)\mathsf{Y}_c}A_{\text{path}}(\mathbf{x}_g(t),\mathbf{v}_g(t))\hat{B}\left(\mathbf{x}_g(0)+\frac{\mathbf{y}_g}{2}\right)\right.$$
$$\left.+\hat{B}\left(\mathbf{x}_g(0)-\frac{\mathbf{y}_g}{2}\right)e^{-i(m_g/\hbar)\mathbf{v}_g(0)\cdot\mathbf{y}_g - i\mathsf{V}_c(0)^T(\mathsf{M}_{cc}/\hbar)\mathsf{Y}_c}A_{\text{path}}(\mathbf{x}_g(t),\mathbf{v}_g(t))\right]\frac{\rho\left[\mathsf{X}(0)+\frac{\mathsf{Y}}{2},\mathsf{X}(0)-\frac{\mathsf{Y}}{2}\right]}{Q}, \tag{3.26}$$

where $\mathsf{Y}\equiv\mathsf{R}_3-\mathsf{R}_1$. In this last equation, $A_{\text{path}}(\mathbf{x}_g(t),\mathbf{v}_g(t))$ is the function defined by the operator $\hat{A}$ which is evaluated in terms of the guest and target final position and velocities which are obtained by solving Eqs. (3.25a), (3.25b), and (3.25c) with the proper initial conditions (these initial conditions are then averaged over with a weight that is prescribed by the density matrix).

Note that Eqs. (3.25a), (3.25b), and (3.25c) are completely deterministic and are identical, modulo the weight on the initial conditions, with the classical equations of motion found in papers I and II. Also, when $\hat{A}$ and $\hat{B}$ are set to one, the Y integrations in Eq. (3.26) simply give the Wigner distribution [40] form of the density matrix.

As was shown earlier by Deutch and Silbey [15], these equations can be transformed to a reduced set of generalized Langevin equations (GLE) after the bath degrees of freedom are projected out. Here, this is done by noting that the equation of motion for the bath, Eq. (3.25c), is easily solved in terms of the bath initial conditions and in terms of a Green's function that couples to the target degrees of freedom. Then, using the fact that the correlations we want to compute depend explicitly only on the guest degrees of freedom and using Eq. (3.9) for the density matrix, we can perform all remaining bath integrals as well as the target Y_t integrals. Following these two operations, Eq. (3.26) is rewritten in terms of a reduced density matrix and the differential equations that are used to calculate $A_{\text{path}}(\mathbf{x}_g(t),\mathbf{v}_g(t))$ reduce to a smaller set of stochastic coupled equations where the target dynamics are governed by a GLE. The anticommutator correlation then becomes

$$\frac{1}{2}\langle\{\hat{A}(t),\hat{B}\}\rangle = \frac{1}{2}\left(\frac{m_g}{2\pi\hbar}\right)^3 \int d\mathbf{x}_g(0)d\mathbf{v}_g(0)d\mathbf{y}_g d\mathsf{X}_t(0)d\mathsf{V}_t(0)\left[e^{-i(m_g/\hbar)\mathbf{v}_g(0)\cdot\mathbf{y}_g}A_{\text{path}}(\mathbf{x}_g(t),\mathbf{v}_g(t))\hat{B}\left(\mathbf{x}_g(0)+\frac{\mathbf{y}_g}{2}\right)\right.$$
$$\left.+\hat{B}\left(\mathbf{x}_g(0)-\frac{\mathbf{y}_g}{2}\right)e^{-i(m_g/\hbar)\mathbf{v}_g(0)\cdot\mathbf{y}_g}A_{\text{path}}(\mathbf{x}_g(t),\mathbf{v}_g(t))\right]\rho'_g(\mathbf{x}_g(0),\mathbf{y}_g)\rho_{t|g}(\mathsf{X}_t(0),\mathsf{V}_t(0);\mathbf{x}_g(0)), \tag{3.27}$$

where

$$\rho'_g(\mathbf{x}_g(0),\mathbf{y}_g) \equiv \frac{\det\left(\frac{\Xi(\mathsf{D})}{(\Lambda(\mathsf{D})-\Xi(\mathsf{D}))}\right)\exp\left(-\beta V(\mathbf{x}_g(0),\mathsf{R}_t^{(0)}) - \frac{m_g y_g^2}{2\beta\hbar^2} - \frac{\beta}{2}(\mathsf{R}_t^{(0)})^T\mathsf{K}_{\text{eff}}\mathsf{R}_t^{(0)}\right)}{\int d\mathbf{x}_g(0)\det\left(\frac{\Xi(\mathsf{D})}{(\Lambda(\mathsf{D})-\Xi(\mathsf{D}))}\right)\exp\left(-\beta V(\mathbf{x}_g(0),\mathsf{R}_t^{(0)}) - \frac{\beta}{2}(\mathsf{R}_t^{(0)})^T\mathsf{K}_{\text{eff}}\mathsf{R}_t^{(0)}\right)}, \tag{3.28}$$

with $\mathsf{R}_t^{(0)}$ obtained from Eq. (3.8) for $\mathbf{x}_g(0)=\mathbf{r}_g^{(0)}$, and

$$\rho_{t|g}(\mathsf{X}_t(0),\mathsf{V}_t(0);\mathbf{x}_g(0)) \equiv \left\{\det\left[\frac{1}{\pi^2}\left(\mathsf{G}_{tt}(\mathsf{D})-\mathsf{G}_{tb}(\mathsf{D})\frac{1}{\mathsf{G}_{bb}(\mathsf{D})}\mathsf{G}_{bt}(\mathsf{D})\right)\left(\mathsf{H}_{tt}(\mathsf{D})-\mathsf{H}_{tb}(\mathsf{D})\frac{1}{\mathsf{H}_{bb}(\mathsf{D})}\mathsf{H}_{bt}(\mathsf{D})\right)\right]\right\}^{1/2}$$
$$\times\exp\left[-(\mathsf{X}_t(0)-\mathsf{R}_t^{(0)})^T\left(\mathsf{G}_{tt}(\mathsf{D})-\mathsf{G}_{tb}(\mathsf{D})\frac{1}{\mathsf{G}_{bb}(\mathsf{D})}\mathsf{G}_{bt}(\mathsf{D})\right)(\mathsf{X}_t(0)-\mathsf{R}_t^{(0)})\right.$$
$$\left.-\mathsf{V}_t(0)^T\left(\mathsf{H}_{tt}(\mathsf{D})-\mathsf{H}_{tb}(\mathsf{D})\frac{1}{\mathsf{H}_{bb}(\mathsf{D})}\mathsf{H}_{bt}(\mathsf{D})\right)\mathsf{V}_t(0)\right], \tag{3.29}$$

where the subscripts on these matrices indicate the appropriate $t/b,t/b$ blocks, and where we have introduced two new matrices

$$\mathsf{G}(\mathsf{D}) \equiv \hbar^{-1}[\Lambda(\mathsf{D})-\Xi(\mathsf{D})] \tag{3.30a}$$

and

$$\mathsf{H}(\mathsf{D}) \equiv \hbar^{-1}\mathsf{M}\left(\frac{1}{\Lambda(\mathsf{D})+\Xi(\mathsf{D})}\right)\mathsf{M}. \tag{3.30b}$$

In Eq. (3.27), the $\mathbf{x}_g(0)$ dependence of $\rho_{t|g}[\mathsf{X}_t(0),\mathsf{V}_t(0);\mathbf{x}_g(0)]$ comes from the matrices $\mathsf{G}(\mathsf{D})$ and $\mathsf{H}(\mathsf{D})$ as well as from $\mathsf{R}_t^{(0)}$. We have separated the density matrix into two parts in order to highlight the fact that $\rho_{t|g}[\mathsf{X}_t(0),\mathsf{V}_t(0);\mathbf{x}_g(0)]$ can be used as a (conditional) distribution function for the initial target positions and velocities [see Eq. (3.29)] that is easily shown to reduce to the classical equilibrium distribution function for high temperatures. It is easy to show that, when $\hat{A}$ and $\hat{B}$ are both unit operators, the anticommutator, (3.27) is, as expected, also unity.

The reduced set of differential equations that has to be solved in order to obtain $A_{\text{path}}(\mathbf{x}_g(t),\mathbf{v}_g(t))$ is expressed as a set of generalized Langevin equations, i.e.,

$$m_g\frac{d^2\mathbf{x}_g}{dt^2} = \mathbf{F}_g(\mathbf{x}_g,\mathsf{X}_t) \tag{3.31}$$

and

$$\mathsf{M}_{tt}\frac{d^2\mathsf{X}_t}{dt^2} = \mathsf{F}_t(\mathbf{x}_g,\mathsf{X}_t) - \mathsf{K}_{\text{eff}}\mathsf{X}_t - \int_0^\tau ds\, \mathsf{M}_{tt}^{1/2}\tilde{\mathsf{K}}_{tb} \times \frac{\cos[\tilde{\mathsf{K}}_{bb}^{1/2}(\tau-s)]}{\tilde{\mathsf{K}}_{bb}}\tilde{\mathsf{K}}_{bt}\mathsf{M}_{tt}^{1/2}\dot{\mathsf{X}}_t(s) + \Upsilon^\dagger(\tau), \tag{3.32}$$

where

$$\Upsilon^\dagger(\tau) \equiv -\mathsf{M}_{tt}^{1/2}\tilde{\mathsf{K}}_{tb}\cos(\tilde{\mathsf{K}}_{bb}^{1/2}\tau)\left[\frac{1}{\tilde{\mathsf{K}}_{bb}}\tilde{\mathsf{K}}_{bt} - \frac{1}{\tilde{\mathsf{G}}_{bb}(\mathsf{D})}\tilde{\mathsf{G}}_{bt}(\mathsf{D})\right] \times \mathsf{M}_{tt}^{1/2}[\mathsf{X}_t(0)-\mathsf{X}_t^{(0)}] + \mathsf{M}_{tt}^{1/2}\tilde{\mathsf{K}}_{tb}\frac{\sin(\tilde{\mathsf{K}}_{bb}^{1/2}\tau)}{\tilde{\mathsf{K}}_{bb}^{1/2}}\frac{1}{\tilde{\mathsf{H}}_{bb}(\mathsf{D})} \times \tilde{\mathsf{H}}_{bt}(\mathsf{D})\mathsf{M}_{tt}^{1/2}\mathsf{V}_t(0) + \mathcal{F}^\dagger(\tau), \tag{3.33}$$

and where $\mathcal{F}^\dagger(\tau)$ is a Gaussian random force with zero mean and covariance

$$\langle\mathcal{F}^\dagger(\tau)\mathcal{F}^\dagger(\tau')^T\rangle = \frac{\mathsf{M}_{tt}^{1/2}\tilde{\mathsf{K}}_{tb}}{2}\left(\cos(\tilde{\mathsf{K}}_{bb}^{1/2}\tau)\frac{1}{\tilde{\mathsf{G}}_{bb}(\mathsf{D})}\cos(\tilde{\mathsf{K}}_{bb}^{1/2}\tau') + \frac{\sin(\tilde{\mathsf{K}}_{bb}^{1/2}\tau)}{\tilde{\mathsf{K}}_{bb}^{1/2}}\frac{1}{\tilde{\mathsf{H}}_{bb}(\mathsf{D})}\frac{\sin(\tilde{\mathsf{K}}_{bb}^{1/2}\tau')}{\tilde{\mathsf{K}}_{bb}^{1/2}}\right)\tilde{\mathsf{K}}_{bt}\mathsf{M}_{tt}^{1/2}. \tag{3.34}$$

These expressions are very similar to the ones in I and II (on average, they are, of course, identical to the classical equations of motion); the differences are in the terms denoted by $\Upsilon^\dagger(\tau)$. The ones containing the factors $[\mathsf{X}_t(0)-\mathsf{R}_t^{(0)}]$ and $\mathsf{V}_t(0)$ are completely absent in the classical case. Indeed, a careful analysis of the $\mathsf{G}(\mathsf{D})$ and $\mathsf{H}(\mathsf{D})$ matrices shows that these terms vanish in the high temperature limit. Although these new terms look strange at first glance because the dynamics of the target seems to "remember" the initial positions and velocities through them, we show in Ref. [41] that, when the formalism is used to calculate target-target correlations in the absence of the guest, the resulting correlations are "exact." Furthermore, these two new terms can be considered, such as $\mathcal{F}^\dagger(\tau)$, as colored Gaussian noise since the target initial positions and velocities are randomly sampled from $\rho_{t|g}(\mathsf{X}_t(0),\mathsf{V}_t(0);\mathbf{x}_g(0))$, although they are obviously correlated to the initial positions and velocities.

The random force term in Eq. (3.32), $\mathcal{F}^\dagger(\tau)$, also appears in the classical GLE in papers I and II, albeit with different correlations, see Eq. (3.34). Note that the source of the noise solely arises from the sampling of the bath initial conditions, which is determined by $\mathsf{G}(\mathsf{D})$ and $\mathsf{H}(\mathsf{D})$. It is also easy to show that these correlations identically reproduce the classical generalized Einstein-Nyquist relation in the high-temperature limit; specifically, in the classical limit, the random force correlations are proportional to the memory function

$$\lim_{T\to\infty}\langle\mathcal{F}^\dagger(\tau)^T\mathcal{F}^\dagger(\tau')\rangle = k_B T\mathsf{M}_{tt}^{1/2}\tilde{\mathsf{K}}_{tb}\frac{\cos(\tilde{\mathsf{K}}_{bb}^{1/2}(\tau-\tau'))}{\tilde{\mathsf{K}}_{bb}}\tilde{\mathsf{K}}_{bt}\mathsf{M}_{tt}^{1/2}. \tag{3.35}$$

Hence, while classically the generalized Einstein-Nyquist relation predicts that the noise vanishes at absolute zero, Eq. (3.34) shows that the noise remains finite at very low temperature; this is expected because of zero-point motion.

To summarize, the differential equations, Eq. (3.32), contain quantum generalizations to the classical equations of motion obtained in papers I and II and reduce to them in the high-temperature limit. It is probably too strong to interpret them as equations of motion (e.g., they cannot be used to predict the evolution of a wave packet, even in the harmonic case), they are simply differential equations that approximately lead to the correct correlation functions, but that are nonetheless exact for purely harmonic systems.

We conclude this subsection with some remarks on the approximations we made in the above derivation and compare with earlier work. For example, instead of our approximations on the combination of the forward and the backward propagator, one could have obtained each propagator within the semiclassical WKB approximation [24] in the coherent state-representation [42]. This approach was taken by Makri *et al.* [43–46] in the semiclassical evaluation of correlation functions for nonharmonic quantum systems. In short, both this approach and ours are exact for harmonic systems, but in the latter, a classical simulation of the forward trajectories is followed by another simulation for the backward propagators. In both cases, for nonharmonic systems, terms of order $O(\Upsilon^3)$ are neglected in the evaluation of the propagator. The reason we choose our approach is that it requires half the simulation effort (we simulate the forward and backward path integrals at the same time). Also, our stochastic bound-

ary value problem directly reduces to the classical Langevin equation for high temperatures.

C. The permeability revisited

We conclude this section by explicitly showing how the path integral formalism developed above can be used to obtain the anticommutator correlations needed to calculate the space-dependent Onsager diffusion coefficient $D(z)$ and through it, the permeability. The required correlations are just the Kubo averages that appear in Eq. (2.7), and these can be expressed in terms of anti-commutator correlations using Eq. (2.9).

We start with the density-density correlations, $\langle\{\hat{N}(\mathbf{r}_g,t),\hat{N}(\mathbf{r}'_g)\}/2\rangle$. As in papers I and II, we work in the infinite dilution regime and take $\hat{N}(\mathbf{r}_g,t)=\delta(\mathbf{r}_g-\hat{\mathbf{r}}_g(t))$. Because this operator simply multiplies the other factors in Eq. (3.27), we trivially obtain

$$\frac{1}{2}\langle\{\hat{N}(\mathbf{r}_g,t),\hat{N}(\mathbf{r}'_g)\}\rangle = \frac{1}{2}\left(\frac{m_g}{2\pi\hbar}\right)^3 \int d\mathbf{x}_g(0)d\mathbf{v}_g(0)d\mathbf{y}_g d\mathsf{X}_t(0)d\mathsf{V}_t(0)\,\delta(\mathbf{r}_g-\mathbf{x}_g(t))\left[\delta\left(\mathbf{r}'_g-\mathbf{x}_g(0)-\frac{\mathbf{y}_g}{2}\right)+\delta\left(\mathbf{r}'_g-\mathbf{x}_g(0)+\frac{\mathbf{y}_g}{2}\right)\right]$$
$$\times e^{-i(m_g/\hbar)\mathbf{v}_g(0)\cdot\mathbf{y}_g}\rho'_g(\mathbf{x}_g(0),\mathbf{y}_g)\rho_{t|g}(\mathsf{X}_t(0),\mathsf{V}_t(0);\mathbf{x}_g(0)). \tag{3.36}$$

The sum of the two delta functions is then Taylor expanded in $\mathbf{y}_g$. It is easy to show that, when the $\mathbf{y}_g$ integrations are performed, the Taylor expansion in $\mathbf{y}_g$ becomes an expansion in $\hbar$. To be consistent with our density matrix approximation, see Eq. (3.9), we only keep the leading term in the expansion, and Eq. (3.36) becomes

$$\left\langle\frac{\{\hat{N}(\mathbf{r}_g,t),\hat{N}(\mathbf{r}'_g)\}}{2}\right\rangle = \int d\mathbf{x}_g(0)d\mathbf{v}_g(0)d\mathsf{X}_t(0)d\mathsf{V}_t(0)[\delta(\mathbf{r}_g-\mathbf{x}_g(t))\,\delta(\mathbf{r}'_g-\mathbf{x}_g(0))\rho_g(\mathbf{x}_g(0),\mathbf{v}_g(0))\rho_{t|g}(\mathsf{X}_t(0),\mathsf{V}_t(0);\mathbf{x}_g(0))], \tag{3.37}$$

where

$$\rho_g(\mathbf{x}_g(0),\mathbf{v}_g(0)) \equiv \frac{\left(\frac{\beta m_g}{2\pi}\right)^{3/2}\det\left(\frac{\Xi(\mathsf{D})}{(\Lambda(\mathsf{D})-\Xi(\mathsf{D}))}\right)\exp\left\{-\beta\left[\frac{1}{2}m_g v_g(0)^2+V(\mathbf{x}_g(0),\mathsf{R}_t^{(0)})+\frac{1}{2}(\mathsf{R}_t^{(0)})^T\mathsf{K}_{\text{eff}}\mathsf{R}_t^{(0)}\right]\right\}}{\int d\mathbf{x}_g(0)\det\left(\frac{\Xi(\mathsf{D})}{(\Lambda(\mathsf{D})-\Xi(\mathsf{D}))}\right)\exp\left\{-\beta\left[V(\mathbf{x}_g(0),\mathsf{R}_t^{(0)})+\frac{1}{2}(\mathsf{R}_t^{(0)})^T\mathsf{K}_{\text{eff}}\mathsf{R}_t^{(0)}\right]\right\}}, \tag{3.38}$$

which is very similar to the classical distribution function modulo the $\Lambda(\mathsf{D})$ and $\Xi(\mathsf{D})$ matrices which contain the quantum mechanical effects of the lattice vibrations. Note that Eq. (3.38) is essentially Eq. (3.28), but with the $\mathbf{y}_g$ transformed to the initial velocity distribution. In Eq. (3.37), $\mathbf{x}_g(t)$ is obtained by integrating Eq. (3.32) with the noise and initial target parameters sampled from Eqs. (3.34) and (3.29), respectively. The initial position of the guest is fixed at $\mathbf{r}'_g$ and its initial velocity sampled from Eq. (3.38).

As seen from Eq. (2.7), the required correlation $\langle\{\hat{N}(\mathbf{r}_g,t),\hat{N}(\mathbf{r}'_g)\}/2\rangle$, must be evaluated for $t=0$. In this case, $\mathbf{x}_g(t)=\mathbf{r}'_g$ and

$$\frac{1}{2}\langle\{\hat{N}(\mathbf{r}_g),\hat{N}(\mathbf{r}'_g)\}\rangle = \delta(\mathbf{r}_g-\mathbf{r}'_g)\int d\mathbf{v}_g(0)\rho_g(\mathbf{r}_g,\mathbf{v}_g(0))$$
$$= \delta(\mathbf{r}_g-\mathbf{r}'_g)n_{\text{bulk}}e^{-\beta W(\mathbf{r}_g)}, \tag{3.39}$$

where $W(\mathbf{r}_g)$ is the potential of mean force as defined in Eq. (3.15). Note that the δ function is completely expected and the approximate nature of the result is in $W(\mathbf{r}_g)$, see Eq. (3.9). While the full time dependence of $\langle\{\hat{N}(\mathbf{r}_g,t),\hat{N}(\mathbf{r}'_g)\}\rangle$ must be known in order to compute the Kubo average according to Eq. (2.9), we will show below that, at room temperature, the Kubo average and the anticommutator of guest operators are almost indistinguishable, and thus, the equal time Kubo average is also given by the right-hand side of Eq. (3.39).

The remaining two anticommutator correlations that appear in Eq. (2.7) can be obtained by applying the same approximations that led to Eq. (3.39). The details are given in Ref. [41]; here, we simply state the final results, namely,

$$\frac{1}{2}\langle\{\hat{\mathbf{J}}(\mathbf{r}_g,t),\hat{\mathbf{J}}(\mathbf{r}'_g)\}\rangle = \int d\mathbf{x}_g(0)d\mathbf{v}_g(0)d\mathsf{X}_t(0)d\mathsf{V}_t(0)$$
$$\times\delta(\mathbf{r}_g-\mathbf{x}_g(t))\,\delta(\mathbf{r}'_g-\mathbf{x}_g(0))\mathbf{v}_g(t)\mathbf{v}_g(0)$$
$$\times\rho_g(\mathbf{x}_g(0),\mathbf{v}_g(0))\rho_{t|g}(\mathsf{X}_t(0),\mathsf{V}_t(0);\mathbf{x}_g(0)) \tag{3.40}$$

and

$$\frac{1}{2}\langle\{\hat{N}(\mathbf{r}_g,t),\hat{\mathbf{J}}(\mathbf{r}_g')\}\rangle$$
$$= \int d\mathbf{x}_g(0)d\mathbf{v}_g(0)d\mathsf{X}_t(0)d\mathsf{V}_t(0)$$
$$\times\delta(\mathbf{r}_g-\mathbf{x}_g(t))\,\delta(\mathbf{r}_g'-\mathbf{x}_g(0))\mathbf{v}_g(0)$$
$$\times\rho_g(\mathbf{x}_g(0),\mathbf{v}_g(0))\rho_{t|g}(\mathsf{X}_t(0),\mathsf{V}_t(0);\mathbf{x}_g(0)). \tag{3.41}$$

The functional forms of these expressions are again identical to their classical counterparts, although here too, the dynamics, the noise distribution and the initial condition distribution are different from what is obtained classically.

Finally, since the expressions that we obtained for the three necessary anti-commutator correlations have the same properties as the classical correlations, the steps that led to the approximate expression for $D(z)$, see Eq. (2.5), are equally valid. More precisely, the functional forms of our semiclassical $\frac{1}{2}\langle\{\hat{\mathbf{J}}(\mathbf{r}_g,t),\hat{\mathbf{J}}(\mathbf{r}_g')\}\rangle$, $\frac{1}{2}\langle\{\hat{N}(\mathbf{r}_g,t),\hat{\mathbf{J}}(\mathbf{r}_g')\}\rangle$, and $\frac{1}{2}\langle\{\hat{N}(\mathbf{r}_g,t),\hat{N}(\mathbf{r}_g')\}\rangle$ greatly simplifies Eq. (2.7) and, if we again assume $D(z)e^{\beta W(z)}$ to be approximately constant close to the barrier tops (implying that the motion is a Smoluchowki diffusion process in that region), the classical derivation for $D(z)$ goes through unchanged (for more details, see Ref. [3]). Again, the correlations that appear in Eq. (2.7) are Kubo averages and here we have worked with the anticommutator. In order to be consistent, we should apply the transformation (2.9) to the anticommutators before solving Eq. (2.7). On the other hand, because the guest dynamics is slow, we expect the Kubo average and the anticommutator to be approximately equal, as is shown numerically in Sec. V.

IV. COMPUTATIONAL DETAILS

In this section we show how the formalism developed above can be implemented numerically; specifically, we consider two issues: First, the potential of mean force is defined in terms of large matrices that are functions of the harmonic force matrix in the presence of the guest, i.e., $\Lambda(\mathsf{D})$ and $\Xi(\mathsf{D})$ in Eq. (3.15). Here, the effect of the guest is not as simple as in papers I and II because quantum mechanically the guest modifies the bath-bath blocks of these matrices. We will show how we can overcome this problem by using the theory of vibrational defects [47] and some well-chosen contour integrations. Second, we need an efficient procedure to simulate the new random terms that appear in the differential equations, i.e., $\Upsilon^{\dagger}(\tau)$ in Eq. (3.32). We will show that these new terms are easily simulated by implementing a Brillouin zone summation during the simulation process and by using our approximation, which was tested in papers I and II, for the memory function.

A. Potential of mean force

Here, we show how the new terms in the potential of mean force, i.e., $\Delta W(\mathbf{r}_g)$, see Eq. (3.16), can be calculated. These terms are most easily written in terms of the vibrational normal modes of the crystal

$$\Delta W(\mathbf{r}_g) = k_B T\sum_{j=1}^{3N}(f(\omega_j')-f(\omega_j)), \tag{4.1}$$

with

$$f(\omega) \equiv \frac{\beta\hbar\omega}{2} + \ln(1-e^{-\beta\hbar\omega}), \tag{4.2}$$

and where ω_j' is the jth normal mode frequency of the lattice in the presence of the frozen guest [i.e., where D is added to K, see Eqs. (3.10) and (3.11)], ω_j is the jth normal frequency of the pure lattice ($\mathsf{D}=0$), and N is the number of atoms in the crystal.

We can reexpress Eq. (4.1) as a contour integral as

$$\beta\Delta W(\mathbf{r}_g) = \sum_{j=1}^{3N}\frac{1}{i\pi}\oint_{C1} d\omega\,\omega f(\omega)\left(\frac{1}{\omega^2-\omega_j'^2}-\frac{1}{\omega^2-\omega_j^2}\right), \tag{4.3}$$

where $C1$ is a counter clockwise contour that includes all positive poles of the integrand and that excludes the logarithmic branch cut that lies on the negative real axis. From here, it is easy to show that $\Delta W(\mathbf{r}_g)$ can be written in terms of the vibrational Green's function of the crystal

$$\beta\Delta W(\mathbf{r}_g) = \frac{1}{i\pi}\oint_{C1} d\omega\,\omega f(\omega)\mathrm{Tr}[\mathcal{G}(\omega,\mathsf{D})-\mathcal{G}(\omega,0)], \tag{4.4}$$

where Tr is a trace and where the Green's function matrices are defined by

$$\mathcal{G}(\omega,\mathsf{D}) \equiv \frac{1}{\omega^2-\tilde{\mathsf{K}}-\tilde{\mathsf{D}}} \tag{4.5}$$

[$\mathcal{G}(\omega,0)$ is the original Green's function of the pure crystal]. The advantage of writing $\Delta W(\mathbf{r}_g)$ in terms of the Green's function is that we can use the theory of defects, as we did in paper I, to compute the trace using matrices that are defined in the target subspace only. Specifically, as was shown in paper I, $\mathcal{G}(\omega,\mathsf{D})$ can be calculated in terms of the perfect lattice Green's function $\mathcal{G}(\omega,0)$ as

$$\mathcal{G}(\omega,\mathsf{D}) = \begin{pmatrix} (1-\mathcal{G}_{tt}(\omega,0)\tilde{\mathsf{D}})^{-1}\mathcal{G}_{tt}(\omega,0) & (1-\mathcal{G}_{tt}(\omega,0)\tilde{\mathsf{D}})^{-1}\mathcal{G}_{tb}(\omega,0) \\ \mathcal{G}_{bt}(\omega,0)\tilde{\mathsf{D}}(1-\mathcal{G}_{tt}(\omega,0)\tilde{\mathsf{D}})^{-1}\mathcal{G}_{tt}(\omega,0)+\mathcal{G}_{bt}(\omega,0) & \mathcal{G}_{bt}(\omega,0)\tilde{\mathsf{D}}(1-\mathcal{G}_{tt}(\omega,0)\tilde{\mathsf{D}})^{-1}\mathcal{G}_{tb}(\omega,0)+\mathcal{G}_{bb}(\omega,0) \end{pmatrix}. \tag{4.6}$$

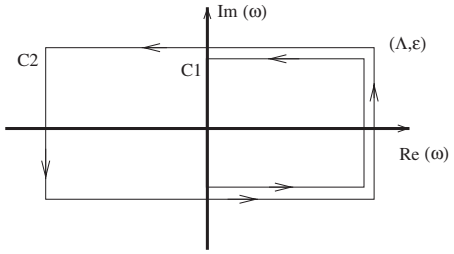

FIG. 2. The two contours $C1$ and $C2$ described in the text, are illustrated in the complex ω plane. Here, the absolute value of the real part of ω is bounded by Λ and the absolute value of the imaginary part is bounded by ε.

What we really need in order to compute $\Delta W(\mathbf{r}_g)$ is the trace of the difference between $\mathcal{G}(\omega,\mathsf{D})$ and $\mathcal{G}(\omega,0)$, and using the last equation and the invariance of the trace under cyclic permutations, we finally obtain

$$\beta\Delta W(\mathbf{r}_g) = \frac{1}{i\pi}\oint_{C1} d\omega\, \omega f(\omega)\mathrm{Tr}[(\mathcal{G}^2(\omega,0))_{tt} \times \tilde{\mathsf{D}}(1-\mathcal{G}_{tt}(\omega,0)\tilde{\mathsf{D}})^{-1}], \tag{4.7}$$

where

$$(\mathcal{G}^2(\omega,0))_{tt} = (\mathcal{G}_{tt}(\omega,0)\mathcal{G}_{tt}(\omega,0) + \mathcal{G}_{tb}(\omega,0)\mathcal{G}_{bt}(\omega,0)) \tag{4.8}$$

is the tt block of $\mathcal{G}(\omega,0)^2$. We show the contour, $C1$, that is used to calculate $\Delta W(\mathbf{r}_g)$ in Fig. 2. Note that the maximum of $\mathrm{Re}(\omega)$ along the contour (Λ in Fig. 2) must be larger than the largest frequency in the crystal vibrational density of states.

The knowledge of the Green's function allows us to compute more than the potential of mean force. In fact, in order to perform the simulations described above, we also need the $\mathsf{G}(\mathsf{D})$ and $\mathsf{H}(\mathsf{D})$ matrices that characterize the distribution of target initial positions and velocities, cf. Eq. (3.29). These matrices satisfy

$$\mathsf{G}_{tt}(\mathsf{D}) - \mathsf{G}_{tb}(\mathsf{D})\frac{1}{\mathsf{G}_{bb}(\mathsf{D})}\mathsf{G}_{bt}(\mathsf{D}) = [\mathsf{L}_{tt}(\mathsf{D})]^{-1} \tag{4.9a}$$

and

$$\mathsf{H}_{tt}(\mathsf{D}) - \mathsf{H}_{tb}(\mathsf{D})\frac{1}{\mathsf{H}_{bb}(\mathsf{D})}\mathsf{H}_{bt}(\mathsf{D}) = [\mathsf{T}_{tt}(\mathsf{D})]^{-1}, \tag{4.9b}$$

and where the two new matrices are defined in the full space as follows:

$$\mathsf{L}(\mathsf{D}) \equiv \mathsf{G}(\mathsf{D})^{-1} \quad \text{and} \quad \mathsf{T}(\mathsf{D}) \equiv \mathsf{H}(\mathsf{D})^{-1}. \tag{4.10}$$

We can also reexpress these matrices in terms of the Green's function and contour integrals; the derivation is very similar to what was done for $\Delta W(\mathbf{r}_g)$ and we simply state the final results for the mass-scaled matrices, namely,

$$\left(\tilde{\mathsf{G}}_{tt}(\mathsf{D}) - \tilde{\mathsf{G}}_{tb}(\mathsf{D})\frac{1}{\tilde{\mathsf{G}}_{bb}(\mathsf{D})}\tilde{\mathsf{G}}_{bt}(\mathsf{D})\right)^{-1} = \frac{2}{\beta\tilde{\mathsf{K}}_{\mathrm{eff}}} + \frac{\hbar}{2\pi i}\oint_{C2} d\omega \coth\left(\frac{\beta\hbar\omega}{2}\right)\mathcal{G}_{tt}(\omega,\mathsf{D}) \tag{4.11}$$

and

$$\left(\tilde{\mathsf{H}}_{tt}(\mathsf{D}) - \tilde{\mathsf{H}}_{tb}(\mathsf{D})\frac{1}{\tilde{\mathsf{H}}_{bb}(\mathsf{D})}\tilde{\mathsf{H}}_{bt}(\mathsf{D})\right)^{-1} = \frac{\hbar}{2\pi i}\oint_{C2} d\omega\, \omega^2 \coth\left(\frac{\beta\hbar\omega}{2}\right)\mathcal{G}_{tt}(\omega,\mathsf{D}), \tag{4.12}$$

where the counterclockwise contour $C2$ shown in Fig. 2, now encloses both positive and negative poles of $\mathcal{G}(\omega,\mathsf{D})$. This can be done because both $\tilde{\mathsf{G}}(\mathsf{D})$ and $\tilde{\mathsf{H}}(\mathsf{D})$ are even functions of ω. Note that in Eq. (4.11), the residue at $\omega=0$ (coming from the hyperbolic cotangent), does not represent any vibrational modes in the crystal and is explicitly canceled by the first term on the right-hand side of Eq. (4.11). Finally, note that the value of the imaginary part of ω along the horizontal parts of the contour, ε in Fig. 2, must satisfy $\varepsilon < \pi/(\beta\hbar)$. This guarantees that the poles of $\coth(\beta\hbar\omega/2)$ that lie on the imaginary axis are excluded from the contour. In practical terms, ε should not be too small because small ε means that the contour passes near the poles on the real axis thereby causing numerical integration problems.

The formalism we just described relies on knowing the Green's function of the perfect crystal in the target space. This was obtained from standard Brillouin zone sums that we briefly review in the next section, but that are extensively described elsewhere (e.g., see Refs. [48,49]).

B. Noise terms

We now consider the noise terms, $\Upsilon^{\dagger}(t)$, in Eq. (3.32). Recall that $\Upsilon^{\dagger}(t)$, not only includes $\mathcal{F}^{\dagger}(t)$, but also the two other nonclassical terms that depend on the initial target positions and velocities. A closer look at Eqs. (3.33) and (3.34) shows that these terms depend on the guest degrees of freedom through the matrices $\mathsf{H}(\mathsf{D})$ and $\mathsf{G}(\mathsf{D})$, and through $\mathsf{R}_t^{(0)}$. Even if this guest dependence is responsible for the temperature dependence of the potential of mean force, its effect on $\mathsf{H}(\mathsf{D})$ and $\mathsf{G}(\mathsf{D})$ is quite small (this was checked by evaluating the guest dependent matrices using the Green's function combined with a contour integration as described in the previous section). Hence, here we will neglect the guest dependence of $\mathsf{H}(\mathsf{D})$ and $\mathsf{G}(\mathsf{D})$ and evaluate the noise terms as if the lattice was perfect. This will allow us to again use Brillouin zone sum techniques.

We start with the $\langle \mathcal{F}^{\dagger}(\tau)^T \mathcal{F}^{\dagger}(\tau')\rangle$ correlations, cf. Eq. (3.34), and perform a double Laplace transform to obtain

$$\mathsf{M}^{-1/2}\langle \mathcal{F}^{\dagger}(s)^T \mathcal{F}^{\dagger}(s')\rangle \mathsf{M}^{-1/2} \approx \frac{1}{2}\tilde{\mathsf{K}}_{tb}\frac{1}{s^2+\tilde{\mathsf{K}}_{bb}}\left(\frac{ss'}{\tilde{\mathsf{G}}_{bb}}+\frac{1}{\tilde{\mathsf{H}}_{bb}}\right)\times\frac{1}{s'^2+\tilde{\mathsf{K}}_{bb}}\tilde{\mathsf{K}}_{bt}, \tag{4.13}$$

where s and s' are the Laplace transform variables and where, for the remainder of this section, we omit the D argument on matrices that are evaluated at $\mathsf{D}=0$. This last relation becomes an equality when G_{bb} and H_{bb} are replaced by $\mathsf{G}_{bb}(\mathsf{D})$ and $\mathsf{H}_{bb}(\mathsf{D})$. This result is not particularly useful because it expresses the noise correlations in terms of matrices in the bath space. Simple matrix manipulations allow us to reexpress this result in terms of matrices in the target space only, i.e.,

$$\mathsf{M}^{-1/2}\langle \mathcal{F}^{\dagger}(s)^T \mathcal{F}^{\dagger}(s')\rangle \mathsf{M}^{-1/2} \approx \frac{1}{\tilde{\mathcal{G}}_{tt}(s)}[\langle \bar{\xi}(s)\bar{\xi}(s')^T\rangle + \langle \bar{\eta}(s)\bar{\eta}(s')^T\rangle]\frac{1}{\tilde{\mathcal{G}}_{tt}(s)}, \tag{4.14}$$

where we have defined two new sets of uncorrelated Gaussian noise vectors of length $3N_{\text{target}}$ (N_{target} is the number of atoms in the target space), $\bar{\xi}(s)$ and $\bar{\eta}(s)$, which have zero mean and variances

$$\langle \bar{\xi}(s)\bar{\xi}(s')^T\rangle \equiv \frac{ss'}{2}\left([\tilde{\mathcal{G}}(s)\tilde{\mathsf{L}}\tilde{\mathcal{G}}(s')]_{tt}-[\tilde{\mathcal{G}}(s)\tilde{\mathsf{L}}]_{tt}\frac{1}{\tilde{\mathsf{L}}_{tt}}[\tilde{\mathcal{G}}(s')\tilde{\mathsf{L}}]_{tt}\right) \tag{4.15}$$

and

$$\langle \bar{\eta}(s)\bar{\eta}(s')^T\rangle \equiv \frac{1}{2}\left([\tilde{\mathcal{G}}(s)\tilde{\mathsf{T}}\tilde{\mathcal{G}}(s')]_{tt}-[\tilde{\mathcal{G}}(s)\tilde{\mathsf{T}}]_{tt}\frac{1}{\tilde{\mathsf{T}}_{tt}}[\tilde{\mathcal{G}}(s')\tilde{\mathsf{T}}]_{tt}\right), \tag{4.16}$$

where the Green's function

$$\tilde{\mathcal{G}}(s) \equiv \frac{1}{s^2+\tilde{\mathsf{K}}} \tag{4.17}$$

is the frequency analytic continuation of Eq. (4.5) for the pure lattice, and where L and T matrices where defined above by Eq. (4.10) with $\mathsf{D}=0$.

The advantage of defining $\bar{\xi}(s)$ and $\bar{\eta}(s)$ in terms of pure lattice matrices is that their respective correlations can be expressed exactly in terms of Brillouin zone sums. For example,

$$\langle \bar{\xi}(s)\bar{\xi}(s')^T\rangle = \frac{1}{2\mathcal{N}}\sum_{\mathbf{k},j}\frac{ss'L[\omega_j(\mathbf{k})]}{(s^2+\omega_j(\mathbf{k})^2)(s'^2+\omega_j(\mathbf{k})^2)}\mathsf{u}_t(\mathbf{k},j)\mathsf{u}_t(\mathbf{k},j)^{\dagger}+\frac{1}{2\mathcal{N}^2}\sum_{\mathbf{k},j}\sum_{\mathbf{k}',j'}\left[\frac{ss'L[\omega_j(\mathbf{k})]L[\omega_{j'}(\mathbf{k}')]}{(s^2+\omega_j(\mathbf{k})^2)(s'^2+\omega_{j'}(\mathbf{k}')^2)}\times\mathsf{u}_t(\mathbf{k},j)\mathsf{u}_t(\mathbf{k},j)^{\dagger}\frac{1}{\tilde{\mathsf{L}}_{tt}}\mathsf{u}_t(\mathbf{k}',j')\mathsf{u}_t(\mathbf{k}',j')^{\dagger}\right], \tag{4.18}$$

where

$$\tilde{\mathsf{L}}_{tt} = \frac{1}{\mathcal{N}}\sum_{\mathbf{k},j} L[\omega_j(\mathbf{k})]\mathsf{u}_t(\mathbf{k},j)\mathsf{u}_t(\mathbf{k},j)^{\dagger}, \tag{4.19}$$

$\mathcal{N}$ is the number of wave numbers used in the discrete sum, $L[\omega_j(\mathbf{k})]=\hbar\coth[\beta\hbar\omega_j/2]/\omega_j$ [as can be obtained combining Eqs. (4.10), (3.30a), (3.30b), (3.10), and (3.11)] and where the sum over j goes from 1 to $3N_{UC}$, where N_{UC} is the number of atoms in the primitive unit cell. In order to have the correct number of vibrational modes, in an exact calculation, $\mathcal{N}$ should be equal to N_c/N_{UC} where N_c is the total number of atoms in the crystal. In practice, $\mathcal{N}$ is much smaller.

The $\omega_j(\mathbf{k})$'s introduced in the last equation are the positive square roots of the eigenvalues of the discrete Fourier transform of the dynamical matrix

$$\tilde{\mathsf{K}}_{n,m}(\mathbf{k}) \equiv \sum_{\mathbf{R}} e^{-i\mathbf{k}\cdot\mathbf{R}}\tilde{\mathsf{K}}_{n,m}(\mathbf{R}), \tag{4.20}$$

where $\tilde{\mathsf{K}}_{n,m}(\mathbf{R})$ is an element of the mass-scaled force constant matrix that couples the nth atom in one unit cell to the mth in another cell, the cells being separated by a lattice vector $\mathbf{R}$. The eigenvectors of $\tilde{\mathsf{K}}(\mathbf{k})$, $\mathsf{e}_j(\mathbf{k})$, define $\mathsf{u}_t(\mathbf{k},j)$ according to

$$[\mathsf{u}_t(\mathbf{k},j)]_m = [\mathsf{e}_j(\mathbf{k})]_n e^{i\mathbf{k}\cdot\mathbf{R}}, \tag{4.21}$$

where n refers to the atom within the primitive unit cell and $\mathbf{R}$ is the translation vector to the actual mth target atom. Since these Brillouin zone sums are real, we can replace $\mathsf{u}_t(\mathbf{k},j)\mathsf{u}_t(\mathbf{k},j)^{\dagger}$ by $\mathrm{Re}(\mathsf{u}_t(\mathbf{k},j)\mathsf{u}_t(\mathbf{k},j)^{\dagger})$ in all of the above expressions.

We now postulate the following form for the noise,

$$\bar{\xi}(s) = \frac{1}{\mathcal{N}} \sum_{\mathbf{k},j} \frac{s}{s^2 + \omega_j(\mathbf{k})^2} \mathrm{Re}(\mathsf{u}_t(\mathbf{k},j)\mathsf{u}_t(\mathbf{k},j)^\dagger) \bar{\xi}_{\mathbf{k},j}, \tag{4.22}$$

where $\bar{\xi}_{\mathbf{k},j}$ is a vector of random variables. In other words, here, the amplitude of each phonon contribution is randomly sampled from a distribution that is appropriately chosen such that Eq. (4.18) is reproduced. It is simple to show that this is accomplished by choosing

$$\langle \bar{\xi}_{\mathbf{k},j} \bar{\xi}^T_{\mathbf{k}',j'} \rangle = \frac{1}{2} \mathcal{N} L[\omega_j(\mathbf{k})] \mathsf{A}_{\mathbf{k},j} \delta_{j,j'} \delta_{\mathbf{k},\mathbf{k}'} - \frac{1}{2} L[\omega_j(\mathbf{k})] L[\omega_{j'}(\mathbf{k}')] \tilde{\mathsf{L}}^{-1}_{tt}, \tag{4.23}$$

where $\mathsf{A}_{\mathbf{k},j}$ is a matrix of rank $3N_{\text{target}}$ defined as

$$\mathsf{B}_{\mathbf{k},j} \mathsf{A}_{\mathbf{k},j} \mathsf{B}_{\mathbf{k},j} \equiv \mathsf{B}_{\mathbf{k},j}, \tag{4.24}$$

where $\mathsf{B}_{\mathbf{k},j} \equiv \mathrm{Re}(\mathsf{u}_t(\mathbf{k},j)\mathsf{u}_t(\mathbf{k},j)^\dagger)$ reproduces $\langle \bar{\xi}(s) \bar{\xi}(s')^T \rangle$ exactly, see Eq. (4.18). Note that Eq. (4.24) is not trivially solved because $\mathsf{B}_{\mathbf{k},j}$ is not invertible. On the other hand, it is easy to show that it has at least one nonzero eigenvalue. Therefore Eq. (4.24) is first transformed to a basis where $\mathsf{B}_{\mathbf{k},j}$ is diagonal, $\mathsf{A}_{\mathbf{k},j}$ is then obtained by solving Eq. (4.24) in the space of nonzero eigenvalues and finally the solution is transformed back to the original space.

The above procedure, when implemented numerically, is memory intensive because it requires the simulation of all the random numbers, $\bar{\xi}_{\mathbf{k},j}$ for all $\mathbf{k}$ and j. Recall that each of these $\bar{\xi}_{\mathbf{k},j}$'s is a vector of length $3N_{\text{target}}$. We can reduce the number of noise variables by considering the scalar $\xi_{\mathbf{k},j} = \mathsf{u}_t(\mathbf{k},j)^\dagger \bar{\xi}_{\mathbf{k},j}$ as the random variable. In general, $\xi_{\mathbf{k},j}$ are complex numbers fully determined by the $\langle \xi_{\mathbf{k},j} \xi^*_{\mathbf{k}',j'} \rangle$ and $\langle \xi_{\mathbf{k},j} \xi_{\mathbf{k}',j'} \rangle$ correlations, which are themselves easily obtained from Eq. (4.23). Using these complex random numbers, we can now write $\bar{\xi}(s)$ as a simple Brillouin zone sum

$$\bar{\xi}(s) = \frac{1}{\mathcal{N}} \sum_{\mathbf{k},j} \frac{s}{s^2 + \omega_j(\mathbf{k})^2} \mathrm{Re}(\mathsf{u}_t(\mathbf{k},j) \xi_{\mathbf{k},j}) \tag{4.25}$$

or equivalently in the time domain

$$\bar{\xi}(t) = \frac{1}{\mathcal{N}} \sum_{\mathbf{k},j} \cos(\omega_j(\mathbf{k}) t) \mathrm{Re}(\mathsf{u}_t(\mathbf{k},j) \xi_{\mathbf{k},j}). \tag{4.26}$$

In practical terms, we simulate all the $\xi_{\mathbf{k},j}$ complex random numbers in advance and we can add the noise variable $\bar{\xi}(t)$ to the equations of motion at any time of the simulation by performing the last Brillouin zone sum, cf. Eq. (4.26).

The same procedure can be applied for $\bar{\eta}(t)$ and gives

$$\bar{\eta}(t) = \frac{1}{\mathcal{N}} \sum_{\mathbf{k},j} \frac{\sin(\omega_j(\mathbf{k}) t)}{\omega_j(\mathbf{k})} \mathrm{Re}(\mathsf{u}_t(\mathbf{k},j) \eta_{\mathbf{k},j}), \tag{4.27}$$

where the $\eta_{\mathbf{k},j} \equiv \mathsf{u}_t(\mathbf{k},j)^\dagger \bar{\eta}_{\mathbf{k},j}$ correlations are obtained, as above, from $\langle \bar{\eta}_{\mathbf{k},j} \bar{\eta}^T_{\mathbf{k}',j'} \rangle$,

$$\langle \bar{\eta}_{\mathbf{k},j} \bar{\eta}^T_{\mathbf{k}',j'} \rangle = \frac{1}{2} \mathcal{N} T(\omega_j(\mathbf{k})) \mathsf{A}_{\mathbf{k},j} \delta_{j,j'} \delta_{\mathbf{k},\mathbf{k}'} - \frac{1}{2} T(\omega_j(\mathbf{k})) T(\omega_{j'}(\mathbf{k}')) \tilde{\mathsf{T}}^{-1}_{tt} \tag{4.28}$$

and, where

$$\tilde{\mathsf{T}}_{tt} \equiv \frac{1}{\mathcal{N}} \sum_{\mathbf{k},j} T(\omega_j(\mathbf{k})) \mathrm{Re}(\mathsf{u}_t(\mathbf{k},j) \mathsf{u}_t(\mathbf{k},j)^\dagger), \tag{4.29}$$

with $T(\omega_j(\mathbf{k})) = \hbar \omega_j \coth(\beta \hbar \omega_j / 2)$.

We now have a formalism that fully reproduces the correlations that appear in the square brackets in Eq. (4.14). We still have to include the effects of the Green's function $\mathcal{G}_{tt}(s)^{-1}$ that multiplies the random variables, cf. Eq. (4.14), but before doing so, we first return to the other random terms that appear in $\Upsilon^\dagger(t)$, namely, the ones that depend on $\mathsf{X}_t(0)$ and $\mathsf{V}_t(0)$ in Eq. (3.33). Again, these terms can be rewritten in terms of matrices in the target space. The matrix manipulations that are performed are quite similar to what we described above and, after a Laplace transform, these terms can be written as $\mathsf{M}^{1/2}_{tt} (\tilde{\mathcal{G}}_{tt}(s))^{-1} \mathcal{Z}(s)$, where

$$\mathcal{Z}(s) \equiv s \left((\tilde{\mathcal{G}}(s) \tilde{\mathsf{L}})_{tt} \frac{1}{\tilde{\mathsf{L}}_{tt}} - (\tilde{\mathcal{G}}(s) \tilde{\mathsf{K}}^{-1})_{tt} \frac{1}{(\tilde{\mathsf{K}}^{-1})_{tt}} \right) \mathsf{M}^{1/2}_{tt} (\mathsf{X}_t(0) - \mathsf{R}^{(0)}_t) + \left((\tilde{\mathcal{G}}(s) \tilde{\mathsf{T}})_{tt} \frac{1}{\tilde{\mathsf{T}}_{tt}} - \tilde{\mathcal{G}}_{tt}(s) \right) \mathsf{M}^{1/2}_{tt} \mathsf{V}_t(0), \tag{4.30}$$

where

$$(\tilde{\mathsf{K}}^{-1})_{tt} = \frac{1}{\mathcal{N}} \sum_{\mathbf{k},j} \frac{1}{\omega_j(\mathbf{k})^2} \mathrm{Re}(\mathsf{u}_t(\mathbf{k},j) \mathsf{u}_t(\mathbf{k},j)^\dagger). \tag{4.31}$$

Clearly $\mathcal{Z}(s)$ can be written in terms of Brillouin zone sums similar to those introduced for $\langle \bar{\xi}(s) \bar{\xi}(s')^T \rangle$ and $\langle \bar{\eta}(s) \bar{\eta}(s')^T \rangle$. Here, we report the final expression in the time domain, i.e.,

$$\mathcal{Z}(t) = \frac{1}{\mathcal{N}} \sum_{\mathbf{k},j} \left\{ \cos(\omega_j(\mathbf{k}) t) \mathrm{Re}(\mathsf{u}_t(\mathbf{k},j) \mathsf{u}_t(\mathbf{k},j)^\dagger) \left[L(\omega_j(\mathbf{k})) \frac{1}{\tilde{\mathsf{L}}_{tt}} - \frac{1}{\omega_j(\mathbf{k})^2 (\tilde{\mathsf{K}}^{-1})_{tt}} \right] \mathsf{M}^{1/2}_{tt} (\mathsf{X}_t(0) - \mathsf{R}^{(0)}_t) + \frac{\sin(\omega_j(\mathbf{k}) t)}{\omega_j(\mathbf{k})} \times \mathrm{Re}(\mathsf{u}_t(\mathbf{k},j) \mathsf{u}_t(\mathbf{k},j)^\dagger) \left[T(\omega_j(\mathbf{k})) \frac{1}{\tilde{\mathsf{T}}_{tt}} - 1 \right] \mathsf{M}^{1/2}_{tt} \mathsf{V}_t(0) \right\}. \tag{4.32}$$

At this point, all the noise terms that appear in $\Upsilon^\dagger(t)$, see Eq. (3.32), are formally written as

$$\Upsilon^\dagger(s) = \mathsf{M}^{1/2}_{tt} (\tilde{\mathcal{G}}_{tt}(s))^{-1} (\mathcal{Z}(s) + \bar{\xi}(s) + \bar{\eta}(s)) \equiv \mathsf{M}^{1/2}_{tt} \left(s^2 + \tilde{\mathsf{K}}_{\text{eff}} + \tilde{\mathsf{K}}_{tb} \frac{s^2}{\tilde{\mathsf{K}}_{bb}(s^2 + \tilde{\mathsf{K}}_{bb})} \tilde{\mathsf{K}}_{bt} \right) \mathcal{Q}(s), \tag{4.33}$$

in Laplace frequency space, where $\mathcal{Q}(s) \equiv \mathcal{Z}(s) + \bar{\xi}(s) + \bar{\eta}(s)$ and where we have obtained the target-target part of $\mathcal{G}_{tt}(s)$ in

terms of the force constant matrix according to Eq. (4.17). Since Eq. (3.32) will eventually be numerically simulated in time, it is convenient to write the noise terms in time; they can be rewritten as

$$\Upsilon^{\dagger}(t) = \mathsf{M}_{tt}^{1/2}\left(\frac{d^2\mathcal{Q}(t)}{dt^2} + \tilde{\mathsf{K}}_{\mathrm{eff}}\mathcal{Q}(t) + \int_0^{\tau} d\tau \tilde{\mathsf{K}}_{tb}\frac{\cos(\tilde{\mathsf{K}}_{bb}^{1/2}(t-\tau))}{\tilde{\mathsf{K}}_{bb}}\tilde{\mathsf{K}}_{bt}\dot{\mathcal{Q}}(\tau)\right), \quad (4.34)$$

where $\mathcal{Q}(0)$ and $\dot{\mathcal{Q}}(0)$ are both zero. In this equation, the memory term

$$\left(\tilde{\mathsf{K}}_{tb}\frac{\cos(\tilde{\mathsf{K}}_{bb}^{1/2}(t-\tau))}{\tilde{\mathsf{K}}_{bb}}\tilde{\mathsf{K}}_{bt}\right)$$

is, up to factors of mass, identical to the memory function appearing in Eq. (3.32) and to that appearing in the classical Langevin equations used in papers I and II.

As was done in papers I and II, we approximate the Laplace transform of the memory function as

$$\tilde{\mathsf{K}}_{tb}\frac{s}{\tilde{\mathsf{K}}_{bb}(s^2+\tilde{\mathsf{K}}_{bb})}\tilde{\mathsf{K}}_{bt} \approx \frac{s}{\tilde{\mathsf{A}}+\tilde{\mathsf{B}}s+\tilde{\mathsf{C}}s^2}, \quad (4.35)$$

where $\tilde{\mathsf{A}}$ and $\tilde{\mathsf{C}}$ are obtained for the small and large s limit of the memory function and where $\tilde{\mathsf{B}}$ is determined from a linear least squares fit (see paper I). In this form, Eq. (4.34) can be simplified by introducing a new field $\mathsf{f}(t)$

$$\Upsilon^{\dagger}(t) = \mathsf{M}_{tt}^{1/2}\left(\frac{d^2\mathcal{Q}(t)}{dt^2} + \tilde{\mathsf{K}}_{\mathrm{eff}}\mathcal{Q}(t) + \frac{d\mathsf{f}(t)}{dt}\right), \quad (4.36)$$

where $\mathsf{f}(t)$ is the solution of the differential equation

$$\tilde{\mathsf{C}}\frac{d^2\mathsf{f}(t)}{dt^2} + \tilde{\mathsf{B}}\frac{d\mathsf{f}(t)}{dt} + \tilde{\mathsf{A}}\mathsf{f}(t) = \frac{d\mathcal{Q}(t)}{dt}, \quad (4.37)$$

with the initial conditions $\mathsf{f}=d\mathsf{f}/dt=0$ at $t=0$. It is easy to show, by Laplace transforming, that the two representations of the noise, i.e., Eqs. (4.36) and (4.34), are equivalent [to the extent that our approximation to the memory function (4.35) is accurate]. Note that the approximation to the memory function (4.35) is also used for the friction term in Eq. (3.32).

We close this section by noting that the only approximations used in the noise term calculation were the use of the approximate memory function, as in papers I and II it reproduces the vibrational density of states semiquantitatively, cf. Fig. 1, and the neglect of the guest position dependence of various matrices. This formalism requires the Brillouin zone sums to be performed while Eq. (3.32) is simulated, and of course, while including more discrete wave numbers improves the accuracy of the noise terms, it also makes the numerical calculation more time consuming.

V. RESULTS

We now apply our formalism to neon in α-quartz. Recall that in papers I and II, we studied, respectively, xenon in the sodalite Theta-1 and argon in α-quartz. In paper I, our conclusions were that the crystal vibrations had very little effects on the guest motion. In paper II, we found the opposite, namely, the crystal vibrations and the flexibility of the lattice played a major role in the diffusion. Part of this was explained by the fact that the channels in Theta-1 are much wider than those in α-quartz, and thus, in α-quartz, the guest is always very close to one or many crystal atoms, with concomitant enhanced coupling between the guest and crystal dynamics. We therefore chose α-quartz again because we expect that any vibrational quantum effects on the guest motion will be larger in systems where the guest-lattice interaction is stronger.

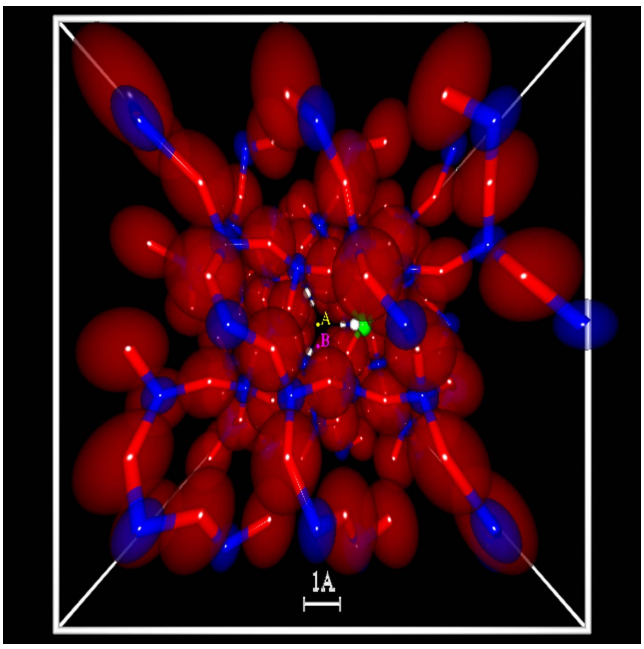

FIG. 3. (Color online) The target zone used in all simulations is shown in the box. Red (light gray) and blue (dark gray) atoms are oxygen and silicon, respectively. The silicon atom whose correlations are reported in Fig. 8 appears in green (light gray sphere directly to the right of the labels A and B). The positions labeled A and B are associated with the potential of mean force results of Fig. 6 and the guest correlations shown in Fig. 9, respectively. The locations of some of the binding sites are shown as small white spheres. In this figure, the z axis is normal to the page.

The spatial group of α-quartz is $P3_121$ and the coordinates of the unit cell were obtained from Ref. [50]. The crystal parameters (atoms positions and harmonic force constants with stretching and bending motion only) are described in paper II. We used the usual Lennard-Jones interaction potentials

$$V(\mathbf{r}_g,\mathsf{R}_t) = \sum_{j=1}^{N_{\mathrm{target}}} 4\epsilon_{j,g}\left[\left(\frac{\sigma_{j,g}}{r_{j,g}}\right)^{12} - \left(\frac{\sigma_{j,g}}{r_{j,g}}\right)^{6}\right], \quad (5.1)$$

where $r_{i,g}$ is the distance between the guest and the jth target atom. As was obtained in papers I and II, the potential parameters are $\epsilon_{O,g}/k_BT=0.1841$, $\epsilon_{Si,g}/k_BT=0.0385$, $\sigma_{O,j}=1.9584$ Å, and $\sigma_{O,j}=2.256$ Å at 300 K, and probably

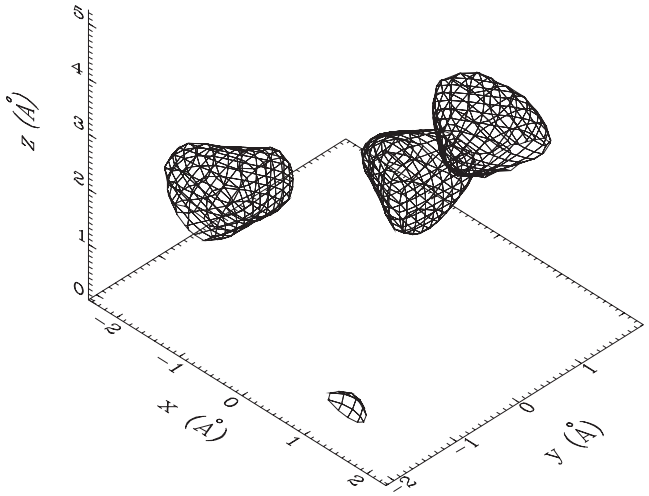

FIG. 4. Potential of mean force energy surface is shown for neon inside α-quartz. The surface is drawn for $W(\mathbf{r}_g)=3.5k_BT$ at 300 K.

give accurate interaction potentials to within a factor of two. The target zone that has dimensions (14.7402 Å, 12.7653 Å, 16.2156 Å), contains 243 atoms, exactly 27 primitive unit cells, and is large enough such that the interaction energy between the guest and bath is practically zero. In this geometry, the crystal is oriented such that the net flow is parallel to the z axis. The target zone that we used in all simulations is shown in Fig. 3.

A. Potential of mean force for neon in α-quartz

We first report the results of the potential of mean force calculation. Recall that the potential of mean force is given by Eqs. (3.15) and (3.16). We computed $\Delta W(\mathbf{r}_g)$ using the contour $C1$ defined in Sec. IV A with $\Lambda=3.56993\times10^{14}$ s^{-1} and $\varepsilon=4.66048\times10^{12}$ s^{-1} (here, Λ is about 30% larger than the largest vibrational frequency of the crystal). The contour integral was performed numerically using

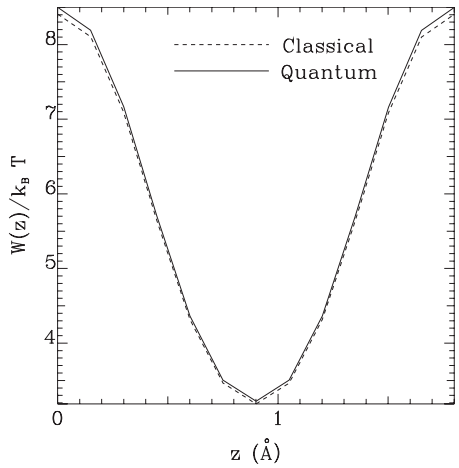

FIG. 5. Plane average potential of mean force is shown for neon inside α-quartz at 300 K. Our semiclassical approximation is compared against the classical expression.

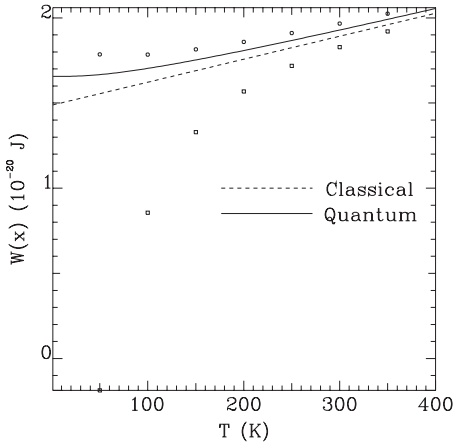

FIG. 6. The potential of mean force of neon inside α-quartz at the point (−0.2305 Å, 0.0 Å, 0.0 Å) is shown as a function of temperature. The two sets of points are obtained from approximations similar to those in Refs. [30–32]. The points are obtained using reference frequencies that include curvature corrections at either the closest local minimum (circles) or global minimum (squares).

Simpson's rule with $\Delta\omega=4.66048\times10^{11}$ s^{-1}. The Green's function that was used in the contour integration was precalculated with $\mathcal{N}=15^3$ dispersion points in reciprocal space.

A constant potential of mean force surface at 300 K for a region well inside the target zone is shown in Fig. 4. Because of the crystal symmetry, there are three absolute minima in the potential of mean force each with $W_{\min}=-0.97483k_BT$ at 300 K. We do not show the classical counterpart of Fig. 4 because the differences are too small to be seen given the resolution of the figure.

Because the net macroscopic flux is taken to be along the z axis, the theory requires the evaluation of plane-average potential of mean force $W(z)$ according to Eq. (2.6). This is shown in Fig. 5 where it is compared against the fully classical $W(z)$. The differences between the classical and semiclassical $W(z)$ is very small at 300 K.

As we will see below, these differences will grow as the temperature is lowered, although our approximations, which treat the guest as a free particle, becomes more problematic. The fact that, at least at 300 K, the quantum corrections to the potential of mean force are small already suggest that the corrections to the permeability will not be dramatic. Remember that, the permeability is obtained from $D(z)$ whose dominant contribution comes from the potential of mean force that appears in the exponential. The remaining parts of $D(z)$, which are determined from the evaluation of microscopic correlation functions, will only introduce preexponential corrections.

We now consider the full temperature dependence for the potential of mean force $W(\mathbf{r}_g)$ at a point chosen to be close to that of the minimum energy in the barrier top plane, specifically at $\mathbf{r}_g=(-0.2305\text{ Å}, 0.0\text{ Å}, 0.0\text{ Å})^T$ (the point labeled "A" in Fig. 3). The temperature dependence of the potential of mean force for the classical and quantum case are compared in Fig. 6. The quantum calculation includes zero-point motion, and this contribution persists even at very low temperatures. Again, we stress that the guest approximations be-

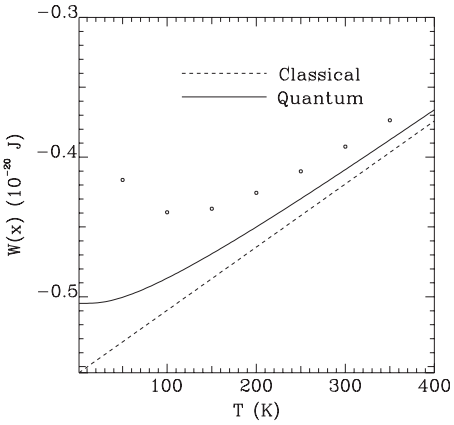

FIG. 7. The potential of mean force of neon inside α-quartz close to a global minimum is shown as a function of temperature. The set of points are obtained from approximations similar to those in Refs. [30–32].

come *ad hoc* at sufficiently low temperatures.

In Fig. 6, we also show a few points for which the semiclassical potential of mean force was obtained from an approximate method similar to the one developed by Ermakov, Butayev, and Spiridonov [29] and later improved by Mak and Andersen [30], Cao and Berne [31], and by Chao and Andersen [32]. The details of the calculation for $W(\mathbf{r}_g)$ within this approximation are shown in the Appendix. Briefly, an approximate form for the density matrix of the full system is used. This approximate density matrix is determined by a set of reference vibrational frequencies that are chosen *ad hoc*, it has the right high temperature limit and it becomes
exact for completely harmonic systems (provided the reference frequencies are appropriately chosen). In Fig. 6, two sets of data for the potential of mean force are shown within this approximation for the same point $\mathbf{r}_g=(-0.2305\ \text{Å}, 0.0\ \text{Å}, 0.0\ \text{Å})^T$. The points shown as circles are obtained from reference frequencies determined from the curvature of the potential at a local minimum close to $\mathbf{r}_g$while the squares are obtained from reference frequencies determined from the global minimum of the potential. Clearly, these approximations are justified because, at low temperature, the paths are expected to sample regions around the various minima. Here, the final answer should be an average of the two data sets. Also note that the curvature at $\mathbf{r}_g$ was not used to determine the reference frequencies because, for some cases, this could result in imaginary reference frequencies.

In Fig. 7, $W(\mathbf{r}_g)$ is reported for a point close to a global minimum. As in Fig. 6, the discrete data points are obtained from the approximation described in the Appendix. Here, the only choice of approximate harmonic reference potential is taken at the global minimum. The problem with this approximation is that it contains many *ad hoc* steps and there is no obvious reason why it should do better than ours at very low temperature. In this paper, we will report the permeability and calculate the correlations at room temperature 300 K. As seen in Figs. 6 and 7, at that temperature, the difference between both methods is small, henceforth, we use the approximation presented in Sec. III.

B. Guest-free correlations

In Sec. III B, we claimed that the formalism we developed is exact when there is no guest, and as shown in Ref. [41], the exact anticommutator correlations for some target quantities are obtained. Of course, in practical terms, we use the numerical methods described in Sec. IV to simulate these correlations, and here, we show how typical anticommutator correlations are reproduced using our simulation procedure compared with the "exact" result obtained by standard methods. Note that the only sources of error here come from our approximation for the memory function, cf. Eq. (4.35), from the numerical methods associated with the integrator, from the limited number of terms used in the Brillouin zone sum, and from the statistical error associated with the finite number of ensemble members used.

We performed our guest-free simulation using a time step of 2.5×10^{-16} s with a second order stochastic Runge-Kutta

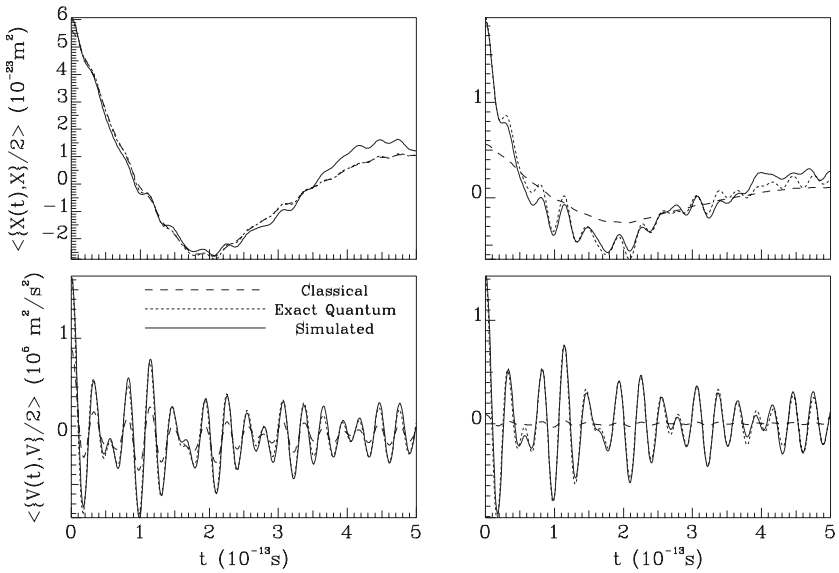

FIG. 8. The anticommutator correlations $\left\langle \frac{\{\hat{X}_1(t),\hat{X}_1\}}{2} \right\rangle$ and $\left\langle \frac{\{\hat{V}_1(t),\hat{V}_1\}}{2} \right\rangle$ are shown for $T=300$ K (left) and $T=30$ K (right) for the silicon atom in green (light gray sphere) in Fig. 3. In each panel, we show the "exact" anticommutator correlation, our simulated result, and the classical correlations.

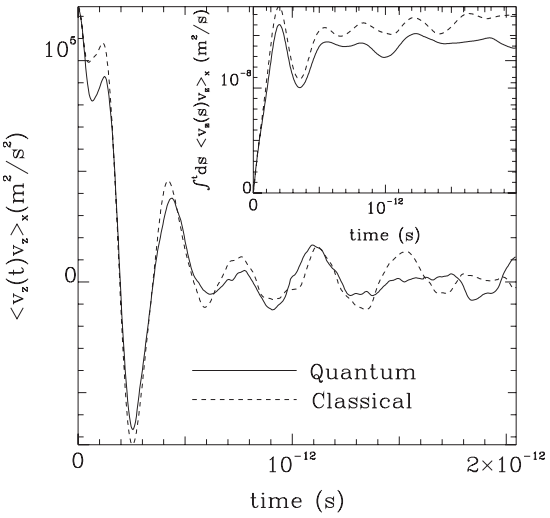

FIG. 9. The simulated velocity-velocity time correlation function for a trajectory where the guest is initially at $\mathbf{x}_g$=(−0.2305 Å,−0.93 Å,0.0 Å) is reported for our semiclassical treatment and for the completely classical case at 300 K. In the inset, we compare the time integral of the same correlation function.

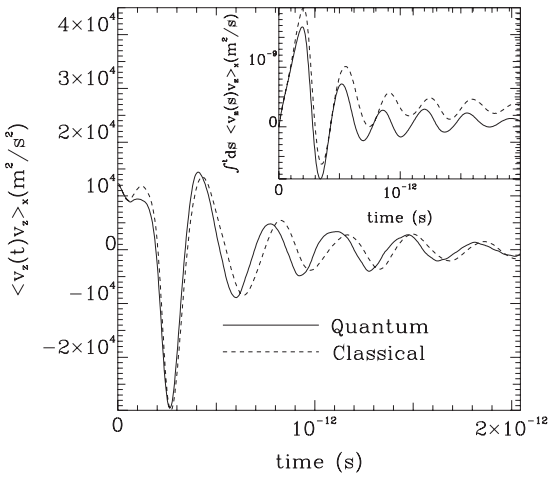

FIG. 10. The simulated velocity-velocity time correlation function for a trajectory where the guest is initially at $\mathbf{x}_g$=(−0.2305 Å,−0.93 Å,0.0 Å) is reported for our semiclassical treatment and for the completely classical case at 30 K. In the inset, we compare the time integral of the same correlation function.

integrator [51] and the noise terms were obtained from Brillouin zone sums with $\mathcal{N}=5^3$. The correlation function was obtained from an ensemble of 2000 trajectories. All simulations reported in this work were performed on a Beowulf cluster containing 64 processors. In Fig. 8, we report $\frac{1}{2}\langle\{\hat{\mathbf{X}}_1(t),\hat{\mathbf{X}}_1\}\rangle$ and $\frac{1}{2}\langle\{\hat{\mathbf{V}}_1(t),\hat{\mathbf{V}}_1\}\rangle$ where the 1 subscript denotes the green silicon atom shown in Fig. 3. These two correlations are shown at 300 and at 30 K. In each panel, the classical correlation is shown for comparison. Figure 8 clearly shows that our simulation procedure and MSR mapping combined with our approximate methods for simulating Eq. (3.32) is very accurate throughout the displayed time window. Except the small error that builds up for the 300 K position correlation at later time, the agreement is still very good for larger times.

As expected, Fig. 8 clearly shows that the quantum corrections are larger at 30 than at 300 K for both types of correlations. Perhaps more interestingly, Fig. 8 also shows that the quantum corrections to the velocity-velocity correlations are noticeably larger than the quantum corrections to the position-position correlations. Even at 300 K, the envelope of the velocity-velocity correlation is about twice as large in the quantum mechanical case, while, at the same temperature, the classical and quantum position-position correlation function only differ slightly.

C. Diffusion and the permeability

We know from Fig. 8 that the quantum corrections to the lattice dynamics are significant even at room temperature. In this section, we examine their coupling to the guest motion. In Fig. 9, we show $\langle v_{G,z}(t)v_{G,z}\rangle_{\mathbf{x}_g(t=0)=\mathbf{r}_g}$ calculated by simulating the GLE (3.32) and averaging over 2000 ensemble members at 300 K, and where we chose $\mathbf{r}_g$=(−0.2305 Å, −0.93 Å,0.0 Å) (a point in the barrier top plane, position "B" in Fig. 3). As above, this was done using a time step of 2.5×10^{-16} s and the noise was obtained from Brillouin zone sums with $\mathcal{N}=5^3$. Note that aging is not necessary in this formalism since the target atoms initial positions are sampled directly from Gaussian distribution given in Eq. (3.29), which includes the relaxation of the lattice to a new equilibrium position. The total length of the simulations was 2.048×10^{-12} s.

As seen from Fig. 9, the quantum mechanical effects on the guest correlations are small, but noticeable. The velocity-velocity correlation function decorrelates faster in the quantum mechanical case, as seen from the faster decrease of the quantum correlations at short time as well as from the lower value of the time integral of the quantum velocity-velocity correlation functions (the inset in Fig. 9). This effect can be explained from the fact that, in the quantum case, the lattice effectively vibrates "more" (the amplitude of the position and velocity correlation functions shown in Fig. 8 are larger in the quantum case). Note that we have shown in paper II that the lattice vibrations tends to slow down the diffusion (i.e., make the velocity autocorrelation function integrals smaller). We believe that the reason these effects are small comes from the guest-free position correlations that are shown in Fig. 8. Remember that, even if the velocity correlations of the quantum lattice is very different compared to the classical lattice at 300 K, the position correlations are not. This means that the actual extent of the motion of the crystal atoms increases in the quantum case, but not by much, at least at 300 K.

When the temperature is dropped to 30 K, the differences become larger. This is shown in Fig. 10 where we again compare $\langle v_{G,z}(t)v_{G,z}\rangle_{\mathbf{x}_g(t=0)=\mathbf{r}_g}$ in the quantum and classical case. Again, the time integral of the velocity correlation function is bigger for the classical calculation. The plateau value of the inset in Fig. 10 is equal to $(1.8199\pm0.46)\times10^{-10}$ m^2/s in the quantum case and $(4.2822\pm0.45)\times10^{-10}$ m^2/s in the classical calculation (also note that both

numbers are about 1 or 2 orders of magnitude below their values at 300 K). Again, for such low temperatures, the classical guest approximation is suspect.

Before going further, recall that the correlation that is shown in Fig. 9 (in the semiclassical approximation) is in fact an anticommutator correlation. On the other hand, the space-dependent diffusion coefficient is given in terms of Kubo averages. Here, we take the anticommutator correlation of Fig. 9 and, from it, we obtain the Kubo average using Eq. (2.9) (using numerical Fourier transforms). The results are shown in Fig. 11. At 300 K, for this system and within the approximation that only the lattice is quantum mechanical, it is clear that the Kubo average and the anticommutator are almost identical. They only differ slightly at short times.This is shown in the inset of Fig. 11. We have also verified that the anticommutator correlation that reduces to $\langle \beta F(z(t_1)) v_{G,z} \rangle_{\mathbf{x}_g(t=0)=\mathbf{r}_g}$ is also almost identical to its Kubo average. Hence, all anticommutator correlations, at this temperature, can be considered to be Kubo averages.

We now examine the space-dependent diffusion coefficient $D(z)$. Recall that $D(z)$ can be obtained from the long-time limit of

$$D(z,t) \equiv \frac{n_\infty \int_0^t dt_1 \int_{\text{unit cell}} d\mathbf{r}_\parallel \langle v_{G,z}(t_1) v_{G,z} \rangle_{\mathbf{x}_g(t=0)=\mathbf{r}_g} e^{-\beta W(\mathbf{r})}}{A_{\text{cell}} + \int_0^t dt_1 \int_{\text{unit cell}} d\mathbf{r}_\parallel \langle \beta F(z(t_1)) v_{G,z} \rangle_{\mathbf{x}_g(t=0)=\mathbf{r}_g} e^{-\beta[W(\mathbf{r})-W(z)]}}, \tag{5.2}$$

where A_{cell} is the area of the primitive unit cell. In Fig. 12, we show how the dynamics (the velocity correlations) changes the region in the plane that contributes to $D(z)$ at 300 K. To do so, we compare the Boltzmann factor $e^{-\beta W(\mathbf{r}_g)}$ against the factor $\int_0^t dt_1 \langle v_{G,z}(t_1) v_{G,z} \rangle_{\mathbf{x}_g(t=0)=\mathbf{r}_g} e^{-\beta W(\mathbf{r}_g)}$ for the quantum case in the maximum energy plane. For each point in the plane, we obtain the required correlation functions through simulations that we described above. The rectangular window that we used to characterize this plane is defined by its lower left corner position (−0.8072 Å, −1.86 Å, 0.0 Å), and its upper right corner position (0.154 Å, 1.86 Å, 0.0 Å). We used a 6×5 grid within this window where, at each grid point, the correlations are explicitly calculated. We then extrapolated between these grid points with a two dimensional bicubic spline. Outside this window, the contribution to $D(z)$ is negligible. Note that, for this plane, $W(z)=8.4997 k_B T$ quantum mechanically and $W(z)=8.4077 k_B T$ classically at 300 K. On the scale of the figure, it is hard to see the differences between the quantum and classical cases, hence, the classical data was not shown. Nonetheless, a careful analysis shows that the contributions to the quantum $D(z)$ are smaller than the classical ones. Also, the region in the plane that contributes to $D(z)$ is slightly narrower in the semiclassical case.

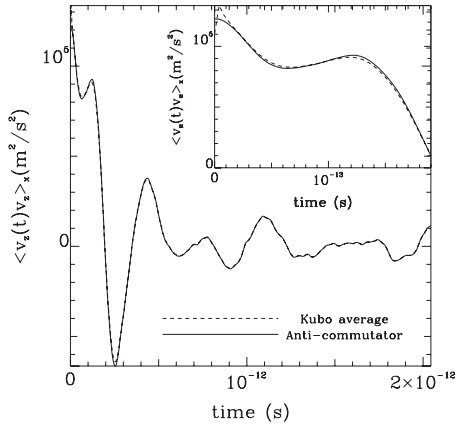

FIG. 11. The anticommutator velocity-velocity correlation shown in Fig. 9, obtained within our semiclassical formalism, is compared with the velocity-velocity Kubo average. The region where the two curves differ the most is shown in the inset.

The factor $D(z,t)/n_\infty e^{-\beta W(z)}$ for the maximum energy plane is shown in Fig. 13, where we also show the uncorrected part of $D(z,t)$, i.e., what is obtained by neglecting the denominator in Eq. (5.2). As expected, Fig. 13 also shows that the quantum corrections to the space dependent diffusion coefficient are not very large, but still make it smaller compared to the classical case. From the plateau value of $D(z,t)/n_\infty e^{-\beta W(z)}$, we can obtain the space dependent diffusion coefficient for that plane. In the quantum case, we find that $D(z,t)/n_\infty e^{-\beta W(z)}=(5.3198 \pm 0.10) \times 10^{-9}$ m^2/s at $z=0$, compared with $(6.1968 \pm 0.14) \times 10^{-9}$ m^2/s classically.

At this point, we assume that $D(z) e^{\beta W(z)}$ to be constant in the barrier region (i.e., the diffusion is a Smoluchowski process) and we calculate the permeability (2.1). We do not test this approximation here as it already was verified classically in papers I and II, and because the semiclassical formalism is much more time consuming numerically. Remember that the goal of this work is to establish the extent of the quantum corrections, if any, on the permeability and for this purpose, the analysis of a single plane is sufficient. With this approximation, we use Eq. (2.1) to calculate the intrinsic permeability and find that $P'(300\ \text{K})=9.91 \times 10^8$ s/(mkg) quantum mechanically, compared with 1.26×10^9 s/(mkg) classically. This predicts that, for this system, the quantum nature of the lattice vibrations decreases the intrinsic permeability by about 25%, with a little less than half the effect coming from

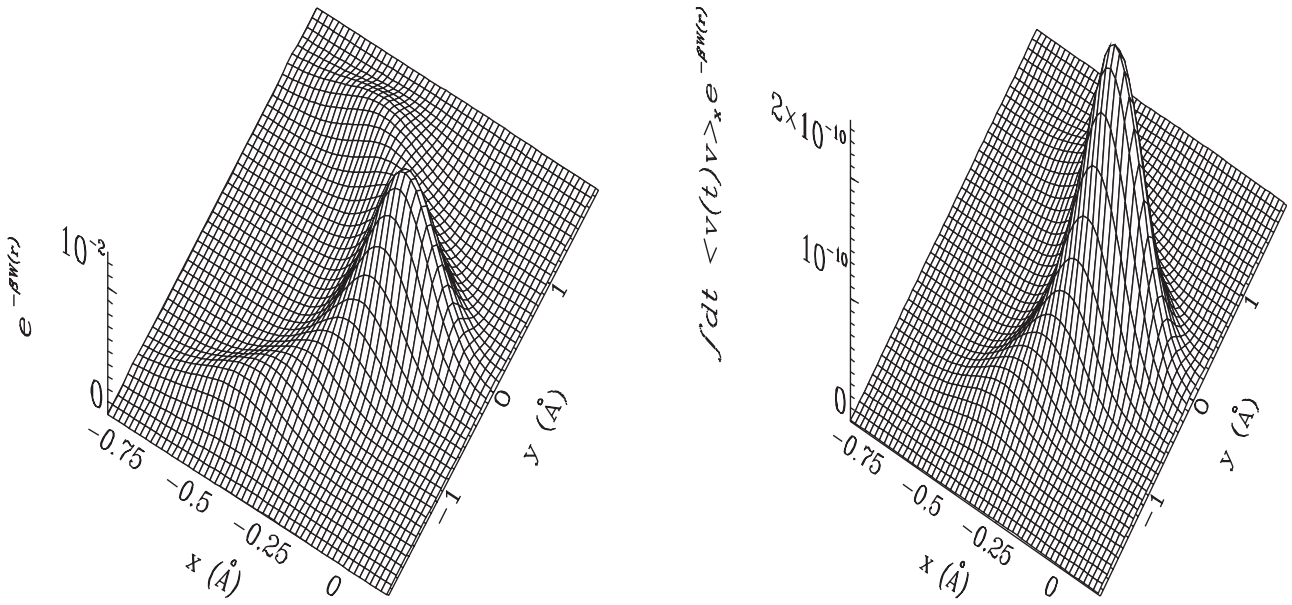

FIG. 12. The Boltzmann factor $e^{-\beta W(\mathbf{r}_g)}$ in the maximum energy plane is compared with $\int_0^t dt_1 \langle v_{G,z}(t_1) v_{G,z} \rangle_{\mathbf{x}_g(t=0)=\mathbf{r}_g} e^{-\beta W(\mathbf{r}_g)}$ at 300 K. The second panel has units of m^2/s.

the potential of mean force and the rest from the velocity correlations. Of course, this result depends strongly on the system under study and even more on the interaction potential that is used.

VI. DISCUSSION

The purpose of this paper was to establish the extent of the first quantum corrections to the guest diffusion in channeled structures. In order to do this, we chose a system for which we have shown classically [2] that the lattice vibrations play a role in the diffusion process. This work was motivated from the well known fact that many crystal phonons are not excited at room temperature, but still have significant zero-point motion contributions.

We have developed a semiclassical formalism where, in effect, the guest is treated classically and the lattice quantum mechanically, based on the MSR relation between stochastic process and path integrals that allowed us to calculate the desired Kubo averages or anticommutator correlations. This formalism, which depends on the fact that the guest is slow, has the advantage that the time correlation function theory of permeability developed earlier by Vertenstein and Ronis [3] remains unchanged formally. More precisely, the connection between the microscopic information, the correlation functions, and the macroscopic permeability is exactly the same as what was used in papers I and II, but now the time correlation functions where obtained from modified generalized Langevin equations and potential of mean force that include the quantum nature of the lattice.

One of the crucial parts of this work is described in Sec. IV. After all, quantum Langevin equations are not new and have been studied for different systems. Here, we gave a very technical procedure that combines Brillouin zone sums techniques and contour integrals such that the new (quantum) terms in the Langevin equations and potential of mean force can be accurately calculated. We also showed how, by using appropriately chosen Gaussian random amplitudes in the Brillouin zone sums, that we could effectively simulate the noise terms in the Langevin equation. This procedure was able to reproduce the guest-free correlation with high accuracy as shown in Fig. 8.

These pure lattice correlation functions show that even at room temperature, the crystal is far from behaving classically. In fact, the velocity-velocity correlations in Fig. 8, in the quantum case, is almost identical at 300 and 30 K, suggesting that at room temperature the velocity of the lattice is

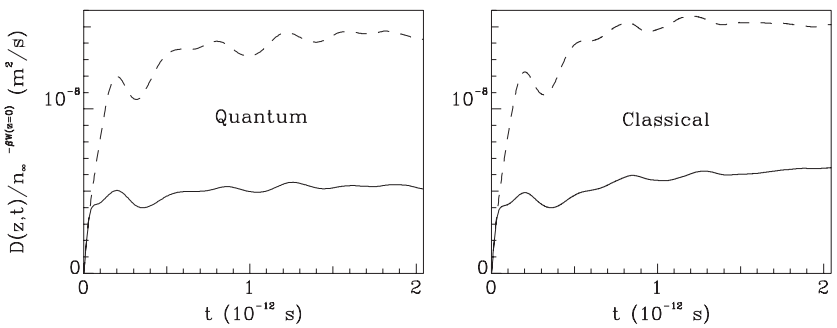

FIG. 13. The quantum space-dependent diffusion coefficient $D(z)$ obtained from the plateau value of the solid curves for the maximum energy plane, $z=0$ is compared with its classical counterpart. The dashed curve represents $D(z,t)$ but where the denominator has been set to 1 in Eq. (5.2).

still dominated by zero-point motion. Moreover, at 300 K, the amplitudes of the velocity-velocity correlations are twice as large in the quantum case. On the other hand, the amplitude of the motion, as characterized by the position-position correlations, does not change drastically, at room temperature, when quantum mechanics is included.

The effects of the quantum lattice were first examined for the potential of mean force. Figures 5 and 6 show that the quantum correction to the potential of mean force are small at room temperature. Still, when the permeability is computed, according to Eq. (2.1), one has to compute $\int_{-d}^{d} dz\, e^{\beta W(z)}$. This integral is a multiple of $\int_{UC} dz e^{\beta W(z)}$, where the "*UC*" subscript means that the integration region is limited to the primitive unit cell along z. For the quantum case, this equals 7.077×10^{-7} m while in the classical case, this gives 6.4323×10^{-7} m at 300 K. The intrinsic permeability is inversely proportional to this factor. Note that small relative quantum corrections to $W(\mathbf{r}_g)$ can be significant when exponentiated if $\beta W(\mathbf{r}_g)$ is large, as seems to be the case here. Hence, at the level of the potential of mean force only, the quantum corrections already decreases the permeability by about 10%.

When the dynamics are included, we get a further decrease in the permeability by another factor of about 15%. This decrease in the diffusion, compared to the classical case, is shown by the plateau value of Fig. 13. This effect is explained by the fact that the lattice effectively vibrates more rapidly in the quantum case. This is in agreement with what we found in paper II where the lattice vibrations slowed down the guest inside the crystal. We also believe that the quantum corrections to the diffusion coefficient are small because the amplitude of the vibrations (the average displacement of each crystal atoms) increases, but only slightly, compared to the classical case.

We have also computed the potential of mean force of argon in α-quartz. In this case, the potential of mean force quantum corrections to the permeability decreases the latter by about 25%. We did perform a limited number of simulations for this case and obtained the velocity time correlation function $\langle v_{G,z}(t) v_{G,z} \rangle_{\mathbf{x}_g(t=0)=\mathbf{r}_g}$ for some points, although not enough to be able to compute $D(z)$. It seems that the dynamical quantum corrections to the permeability is very small for the heavier argon atom.

In conclusions, for the neon and α-quartz systems, both the potential of mean force and the dynamics work in the same direction and ultimately decrease the crystal permeability to neon at room temperature. The total decrease is about 25%. The quantum corrections to the activated free energies or the preexponential dynamical factors are rationalized as follows. In this semiclassical formalism, the lattice effectively vibrates more which further constrains the motion of the guest in an already narrow channel. This extra confinement of the guest manifest itself in larger absolute energies and slower dynamics. Two effects that reduce the permeability.

ACKNOWLEDGMENTS

We thank the McGill's Center for the Physics of Materials for the use of the Beowulf cluster and, in particular, Dr. Juan Gallego for helping us with several parallel processing issues. We also thank the Natural Sciences and Engineering Research Council of Canada for supporting this work. Finally, one of us (B.P.) would also like to thank the *Fonds de recherche sur la nature et les technologies* for support.

APPENDIX: AN ALTERNATE APPROXIMATION FOR $W(\mathbf{x}_g)$

In this approximation, the potential is written as follows:

$$U = V(\mathbf{r}_g^{(1)}, \mathsf{R}_t^{(1)}) + \frac{1}{2}\mathsf{R}_t^{(1)T}\mathsf{K}_{\mathrm{eff}}\mathsf{R}_t^{(1)} + \frac{1}{2}(\mathsf{R} - \mathsf{R}^{(1)})^T\mathsf{K}'(\mathsf{R} - \mathsf{R}^{(1)}) + \delta U, \tag{A1}$$

where the one superscript now refers to the position of a minimum (global or local) of the total potential

$$\mathsf{K}' \equiv \mathsf{K} + \mathsf{D}^{(1)} \tag{A2}$$

and $\mathsf{D}^{(1)}$ is the full matrix of curvatures of V at the minimum (it only has nonzero gg, gt, tg, and tt blocks).

Clearly, if the potential is completely harmonic, δU is zero. Here, we choose δU such that, in the high temperature limit, we obtain our usual classical approximation for the potential of mean force. Hence, we write

$$\begin{aligned}\delta U \equiv{}& V(\mathbf{r}_g, \mathsf{R}_t^{(0)}) - V(\mathbf{r}_g^{(1)}, \mathsf{R}_t^{(1)}) - \frac{1}{2}[(\mathbf{r}_g - \mathbf{r}_g^{(1)})^T\mathsf{D}_{gg}^{(1)}(\mathbf{r}_g - \mathbf{r}_g^{(1)}) \\ &+ 2\mathsf{R}_t^{(0)T}(\mathsf{K}_{\mathrm{eff}} + \mathsf{D}_{tt}^{(0)})(\mathsf{R}_t^{(0)} - \mathsf{R}_t^{(1)}) + \mathsf{R}_t^{(1)T}\mathsf{D}_{tt}^{(0)}\mathsf{R}_t^{(1)} \\ &- \mathsf{R}_t^{(0)T}\mathsf{D}_{tt}^{(0)}\mathsf{R}_t^{(0)}] + \frac{1}{2}(\mathsf{R}_t - \mathsf{R}_t^{(1)})^T(\mathsf{D}_{gg}^{(0)} - \mathsf{D}_{gg}^{(1)})(\mathsf{R}_t - \mathsf{R}_t^{(1)}) \\ &- (\mathsf{R}_t - \mathsf{R}_t^{(1)})^T(\mathsf{K}_{\mathrm{eff}} + \mathsf{D}_{tt}^{(0)})(\mathsf{R}_t^{(0)} - \mathsf{R}_t^{(1)}) - (\mathsf{R}_t \\ &- \mathsf{R}_t^{(1)})^T\mathsf{D}_{tg}^{(1)}(\mathbf{r}_g - \mathbf{r}_g^{(1)}),\end{aligned} \tag{A3}$$

and where $\mathsf{R}_t^{(0)}$ is obtained by solving Eq. (3.8) and where $\mathsf{D}_{tt}^{(0)}$ is given by Eq. (3.12). All quantities with a "(1)" superscript are obtained at the minimum while all quantities with a zero superscript refer to the target and bath minimum when the guest is fixed at $\mathbf{r}_g$. With these defined, we postulate the approximate diagonal part of the complex time propagator

$$\begin{aligned}\rho(\mathsf{R},\mathsf{R}) = \det\left(\frac{\mathsf{M}^{1/2}\tilde{\mathsf{K}}'^{1/2}\mathsf{M}^{1/2}}{2\pi\hbar\,\sinh(\beta\hbar\tilde{\mathsf{K}}'^{1/2})}\right)^{1/2} \\ \times\exp\left[-\beta V(\mathbf{r}_g^{(1)}, \mathsf{R}_t^{(1)}) - \frac{\beta}{2}\mathsf{R}_t^{(1)T}\mathsf{K}_{\mathrm{eff}}\mathsf{R}_t^{(1)}\right. \\ \left. - \frac{1}{2}(\mathsf{R} - \mathsf{R}^{(1)})^T\mathsf{F}(\mathsf{D})(\mathsf{R} - \mathsf{R}^{(1)}) - C\delta U\right],\end{aligned} \tag{A4}$$

where

$$\mathsf{F}(\mathsf{D}^{(0)}) \equiv \hbar^{-1}\mathsf{M}^{1/2}\tanh\left(\frac{\beta\hbar\tilde{\mathsf{K}}'^{1/2}}{2}\right)\tilde{\mathsf{K}}'^{1/2}\mathsf{M}^{1/2}. \tag{A5}$$

The additional parameter C in Eq. (A4), must equal β for high temperature, but is otherwise arbitrary. Because the

nonharmonic nature of the potential is mainly governed by the guest, we choose

$$C = \frac{2}{3}\sum_{j=1}^{3} \mathsf{F}_{gj,gj}(\mathsf{D}^{(1)})\frac{1}{\mathsf{D}^{(1)}_{gj,gj}}, \tag{A6}$$

which is similar to what is done in Refs. [30–32]. Note that the choice of reference potential is justified by the fact that, at low temperatures, the path integral is dominated by the paths that spend most of the time near the minimum, no matter what $\mathbf{r}_g$ is.

Using this approximate form for the density matrix, the potential of mean force is obtained using Eq. (3.13), where the reduced density matrix is obtained by integrating Eq. (A4) over the crystal degrees of freedom. When this is done, we obtain

$$\begin{aligned}
\beta W(\mathbf{r}_g) = {} & (\beta - C)V(\mathbf{r}_g^{(1)}, \mathsf{R}_t^{(1)}) + CV(\mathbf{r}_g, \mathsf{R}_t^{(0)}) + (\mathbf{r}_g - \mathbf{r}_g^{(1)})^T\left(\mathsf{F}_{gg} - C\frac{\mathsf{D}^{(1)}_{gg}}{2}\right)(\mathbf{r}_g - \mathbf{r}_g^{(1)}) + C\left(\mathsf{R}_t^{(0)^T}\mathsf{K}_{\text{eff}}\mathsf{R}_t^{(0)} + \mathsf{R}_t^{(0)^T}\frac{\mathsf{D}^{(0)}_{tt}}{2}\mathsf{R}_t^{(0)}\right. \\
& \left. + \mathsf{R}_t^{(1)^T}\frac{\mathsf{D}^{(0)}_{tt}}{2}\mathsf{R}_t^{(1)} - \mathsf{R}_t^{(0)^T}\mathsf{K}_{\text{eff}}\mathsf{R}_t^{(1)} - \mathsf{R}_t^{(0)^T}\mathsf{D}^{(0)}_{tt}\mathsf{R}_t^{(1)}\right) + \beta\mathsf{R}_t^{(1)^T}\frac{\mathsf{K}_{\text{eff}}}{2}\mathsf{R}_t^{(1)} + (\mathbf{r}_g - \mathbf{r}_g^{(1)})^T\left(C\mathsf{D}^{(1)}_{gt}\mathsf{L}_{tt}\mathsf{F}_{tg} + C\mathsf{D}^{(1)}_{gt}\mathsf{L}_{tb}\mathsf{F}_{bg} - \mathsf{F}_{gc}\mathsf{L}_{cc}\mathsf{F}_{cg}\right. \\
& \left. - \frac{C^2}{4}\mathsf{D}^{(1)}_{gt}\mathsf{L}_{tt}\mathsf{D}^{(1)}_{tg}\right)(\mathbf{r}_g - \mathbf{r}_g^{(1)}) + (\mathsf{R}_t^{(0)} - \mathsf{R}_t^{(1)})^T\left(C(\mathsf{K}_{\text{eff}} + \mathsf{D}^{(0)}_{tt})\mathsf{L}_{tt}\mathsf{F}_{tg} + C(\mathsf{K}_{\text{eff}} + \mathsf{D}^{(0)}_{tt})\mathsf{L}_{tb}\mathsf{F}_{bg} - \frac{C^2}{2}(\mathsf{K}_{\text{eff}} + \mathsf{D}^{(0)}_{tt})\mathsf{L}_{tt}\mathsf{D}^{(1)}_{tg}\right) \\
& \times(\mathbf{r}_g - \mathbf{r}_g^{(1)}) - \frac{C^2}{4}(\mathsf{R}_t^{(0)} - \mathsf{R}_t^{(1)})^T(\mathsf{K}_{\text{eff}} + \mathsf{D}^{(0)}_{tt})\mathsf{L}_{tt}(\mathsf{K}_{\text{eff}} + \mathsf{D}^{(0)}_{tt})(\mathsf{R}_t^{(0)} - \mathsf{R}_t^{(1)}) - \frac{1}{2}\ln[\det(\Phi)] - \frac{1}{2}\ln[\det(\Phi^0)] + \frac{1}{2}\ln[\det(\mathsf{F}'_{cc})] \\
& - \frac{1}{2}\ln[\det(\mathsf{F}^0)] + \frac{3}{2}\ln\left(\frac{m_g}{2\pi\beta\hbar^2}\right),
\end{aligned} \tag{A7}$$

where

$$\Phi \equiv \frac{\mathsf{M}^{1/2}\tilde{\mathsf{K}}'^{1/2}\mathsf{M}^{1/2}}{2\pi\hbar\,\sinh(\beta\hbar\tilde{\mathsf{K}}'^{1/2})}. \tag{A8}$$

The matrices with zero superscript, Φ^0 and F^0, are defined in the absence of the guest (in terms of the original force constant matrix) and they live in the crystal space only (hence, their rank is smaller). We have introduced yet another matrix, L_{cc}, that is defined in the crystal space as

$$\mathsf{L}_{cc}^{-1} \equiv \mathsf{F}'_{cc}, \tag{A9}$$

where

$$\mathsf{F}'_{cc} = \mathsf{F}_{cc} + \begin{pmatrix} \frac{C}{2}(\mathsf{D}^{(1)}_{tt} - \mathsf{D}^{(0)}_{tt}) & 0 \\ 0 & 0 \end{pmatrix}. \tag{A10}$$

Note that, for high temperatures, $\mathsf{L}_{tt} = \frac{2}{\beta}(\mathsf{K}_{\text{eff}} + \mathsf{D}^{(1)}_{tt})^{-1}$. Equation (A7) can then be evaluated numerically using contour integral techniques combined with the theory of defects in a way which is very similar to what is described in Sec. IV A.

[1] Benoit Palmieri and David Ronis, Phys. Rev. E **68**, 046127 (2003).
[2] Benoit Palmieri and David Ronis, J. Phys. Chem. B **109**, 21334 (2005).
[3] M. Vertenstein and D. Ronis, J. Chem. Phys. **85**, 1628 (1986).
[4] T. Mosell, G. Schrimpf, C. Hahn, and J. Brickmann, J. Phys. Chem. **100**, 4571 (1996).
[5] T. Mosell, Ge. Schrimpf, and J. Brickmann, J. Phys. Chem. **100**, 4582 (1996).
[6] T. Mosell, G. Schrimpf, and J. Brickmann, J. Phys. Chem. B **101**, 9476 (1997).
[7] V. Mehra, R. Basra, M. Khanna, and C. Chakravarty, J. Phys. Chem. B **103**, 2740 (1999).
[8] S. El Amrani, F. Vigné-Maeder, and B. Bigot, J. Phys. Chem. **96**, 9417 (1992).
[9] Anastasios I. Skoulidas and David S. Scholl, J. Phys. Chem. B **106**, 5058 (2002).
[10] G. Schrimpf, M. Schlenkrich, J. Brickmann, and P. Bopp, J. Phys. Chem. **96**, 7404 (1992).
[11] D. I. Kopelevich and H.-C. Chang, J. Chem. Phys. **114**, 3776 (2001).
[12] P. Demontis, G. B. Suffritti, E. S. Fois, and S. Quartieri, J. Phys. Chem. **96**, 1482 (1992).
[13] G. B. Suffritti, P. Demontis, and G. Ciccotti, J. Chem. Phys. **118**, 3439 (2003).
[14] P. Demontis, G. Suffritti, S. Bordiga, and R. Buzzoni, J. Chem. Soc., Faraday Trans. **91**, 525 (1995).
[15] J. M. Deutch and R. Silbey, Phys. Rev. A **3**, 2049 (1971).

[16] Ryogo Kubo, J. Phys. Soc. Jpn. **12**, 570 (1957).
[17] Eran Rabani and David R. Reichman, Annu. Rev. Phys. Chem. **56** 157 (2005).
[18] M. Vertenstein and D. Ronis, J. Chem. Phys. **87**, 5457 (1987).
[19] H. Mori, Prog. Theor. Phys. **34**, 423 (1965).
[20] R. Zwanzig, *Lectures in Theoretical Physics* (Interscience, New York, 1961), Vol. 3.
[21] N. Wax, *Selected Papers on Noise and Stochastic Processes* (Dover, New York, 1954).
[22] B. J. Berne and G. D. Harp, Adv. Chem. Phys. **17**, 63 (1970).
[23] R. P. Feynman and A. R. Hibbs, *Quantum Mechanics and Path Integrals* (McGraw-Hill, New York, 1965).
[24] L. S. Schulman, *Techniques and Applications of Path Integrations* (Wiley, New York, 1996).
[25] R. P. Feynman and H. Kleinert, Phys. Rev. A **34**, 5080 (1986).
[26] H. Kleinert, *Path Integrals in Quantum Mechanics, Statistics, Polymer Physics and Financial Markets* (World Scientific, Singapore, 2004).
[27] H. Kleinert, Phys. Lett. A **173**, 332 (1993).
[28] Benoit Palmieri and David Ronis, Phys. Rev. E **73**, 061105 (2006).
[29] K. V. Ermakov, B. S. Butayev, and V. P. Spiridonov, Chem. Phys. Lett. **138**, 153 (1987).
[30] C. H. Mak and Hans C. Andersen, J. Chem. Phys. **92**, 2953 (1990).
[31] Jianshu Cao and B. J. Berne, J. Chem. Phys. **92**, 7531 (1990).
[32] Cecilia E. Chao and Hans C. Andersen, J. Chem. Phys. **107**, 10121 (1997).
[33] H. Kleinert and S. V. Shabanov, Phys. Lett. A **200**, 224 (1995).
[34] Kazuhiro Tsusaka, Phys. Rev. E **59**, 4931 (1999).
[35] Albert Schmid, J. Low Temp. Phys. **49**, 609 (1982).
[36] U. Eckern, W. Lehr, A. Menzel-Dorwarth, F. Pelzer, and A. Scmid, J. Low Temp. Phys. **59**, 885 (1990).
[37] P. C Martin, E. D. Siggia, and H. A. Rose, Phys. Rev. A **8**, 423 (1973).
[38] Roderick V. Jensen, J. Stat. Phys. **25**, 183 (1981).
[39] This result is simple to demonstrate for typical velocity and position operators as shown in Ref. [41]. One has to be more careful when the operator $\hat{A}$ contains higher derivatives of Z. Nonetheless, a careful analysis shows that the result still holds.
[40] E. Wigner, Phys. Rev. **40**, 749 (1932).
[41] Benoit Palmieri, Ph.D thesis, McGill University, Montreal, 2007.
[42] Michael F. Herman and Edward Kluk, Chem. Phys. **91**, 27 (1984).
[43] Jiushu Shao and Nancy Makri, J. Phys. Chem. A **103**, 7753 (1999).
[44] Eric Jezek and Nancy Makri, J. Phys. Chem. A **105**, 2851 (2001).
[45] Nancy Makri, J. Phys. Chem. B **106**, 8390 (2002).
[46] Nicholas J. Wright and Nancy Makri, J. Chem. Phys. **119**, 1634 (2003).
[47] A. A. Maradudin, I. M. Lifshitz, A. M. Kosevitch, W. Cochran, and M. J. P. Musgrave, *Lattice Dynamics* (Benjamin, New York, 1969).
[48] A. A. Maradudin, *Theory of Lattice Dynamics in the Harmonic Approximation* (Academic, New York, 1971).
[49] M. Born and K. Huang, *Dynamical Theory of Crystal Dynamics* (Oxford University Press, Oxford, 1968).
[50] H. Schober, D. Strauch, K. Nützel, and B. Dorner, J. Phys.: Condens. Matter **5**, 6155 (1993).
[51] P. E. Kloeden, E. Platen, and H. Schurz, *Numerical Solutions of SDE Through Computer Experiments* (Springer-Verlag, Berlin, 1994).